Worm addendum thickness and gear curvature interference for enveloping cylindrical worm drive with arc-toothed worm

Xinyue Zhu[1], Yaping Zhao[1], Yifei Chi[1], Gongfa Li[2], Xinyuan Chen[2]

[1] Provincial Key Laboratory of Dynamics and Reliability of Mechanical Equipment. Northeastern University, Shenyang 110819, China

[2] The Key Laboratory of Metallurgical Equipment and Control of Ministry of Education, Wuhan University of Science and Technology, Wuhan 430081, China

Corresponding author: Yaping Zhao; E-mail: zhyp_neu@163.com

Abstract

The purpose of this paper is to provide the calculation methods on worm addendum thickness and curvature interference limit line, and find the feasible value range of the technological crossing angle to avoiding addendum sharpening and curvature interference for enveloping cylindrical worm drive with arc-toothed worm. In accordance with the features of the proposed worm, the mathematical models of cutting and working are established. Based on this, the tooth profile geometry of the worm in its axial section and the worm addendum thickness are obtained by geometric analysis and calculation, and then, the feasible value range of the technological crossing angle is given. In virtue of vector rotation and elimination method, the nonlinear equation with one variable for solving the interference limit line is determined. In the process of solving nonlinear equation, the method of geometric construction is used to judge the existence of solutions and provide an initial value for the subsequent iterative calculation. The numerical example results show that with the increases of the technological crossing angle, the interference limit line is close to the boundary line of the conjugate region of the worm pair, and the hazard of curvature interference evident increases. Generally, a smaller value of the technological crossing angle within its available value range can completely avoid the occurrence of the curvature interference.

Key words: cylindrical worm drive, curvature interference, nonlinear equation, worm addendum thickness, differential geometry

1 Introduction

Arc-toothed cylindrical worm drive, which is usually called Niemann worm drive, was proposed by Niemann and Heyer in 1953 and produced in series by the Flender Company in Germany, so it can be also called F-I worm [1].

Niemann worm with concave surface is formed by machining a cylindrical worm blank with a disc-shaped grinding wheel whose generating surface is toroidal [2, 3]. And the corresponding worm gear with convex surface is enveloped by the cylindrical hob whose generating surface is the same as the worm helicoid. Without doubt, Niemann worm has a series of excellent transmission characterizes, such as large bearing capacity and high transmission efficiency [4]. However, in the process of grinding the worm blank, the crossing angle between the axes of the grinding wheel and the worm blank is the leading angle of the worm on its pitch cylinder [5], which causes the instantaneous contact line between the surfaces of the grinding wheel and the worm is a space curve. And inevitably, it makes the worm helicoid very complicated.

Based on this, in 1968, Litvin brought forward a new-type worm by putting the toroidal grinding wheel on a special position to machine the cylindrical worm blank, namely Litvin worm or F-II worm [1, 5]. In comparison with Niemann worm, Litvin worm has two main features during grinding the

worm blank, as follows: (i) the crossing angle is not the leading angle of the worm, it can be selected in a given range. (ii) the contact line between the surfaces of them is a planar curve, more exactly, it is a segment of circular arc in a section of the worm. Obviously, according to its formation mechanism, the worm helicoid machined in this way is easier.

The curvature interference and addendum pointing are the most common phenomena in worm drive, especially for Litvin worm drive, the curvature interference is its inherent defect [5]. Determined by the forming principle of grinding the worm blank, the tooth profile of the worm changes continuously along its spiral surface when grinding the worm blank, and there is a tendency that the addendum changes to tip [6, 7]. Therefore，the worm addendum thickness should be considered first in the design. As for the so-called curvature interference refers to the curvature interference limit line, i.e., the envelope line of the instantaneous contact line family on the generated tooth surface, enters the meshing area of the worm gear tooth surface, which divides the tooth surface into working area and nonworking area [8]. Generally，there are two regions may occur interference on the tooth surface of the worm gear, one is the dedendum, the other is addendum. they are also called undercutting and top cutting [9]. Once the interference occurs, it will not only reduce the bending strength of the tooth root, but also affect the running stability of the worm pair [10].

In consideration of the importance of this problem, Litvin studied the curvature interference limit line with the precise method and the rough method based on the theories of axes and hub lines of meshing [5]. After that, many researchers [11-17] have studied the curvature interference characteristics of the worm drive and constantly explored the simpler method to solve the curvature interference limit line. Among them, the studies of Zhang and Zhao are more in-depth and specific. Taking Niemann worm as the research object, Zhang [11] elaborated the characteristics of curvature interference, especially the influences of the main parameters of the worm pair and the technological parameters of the worm on it. Zhao [13, 14], taking the conical worm as an example, explained the calculation method of the interference limit line, and then applied this method to calculate the interference limit line of Niemann worm [17].

Compared with Niemann worm, Litvin worm has obvious advantages in manufacturing. However, in many published literatures, there are few specific solution methods and detailed numerical simulation data for curvature interference and addendum sharpening of Litvin worm, and there is no clear explanation on how to avoid these problems. There is no doubt that these will hinder the popularization and application of this kind of worm.

In this paper, based on differential geometry, the calculation formulae of the worm addendum thickness and curvature interference limit line are strictly derived. The tooth profile geometry of the worm in its axial section and the nonlinear equation with one variable for solving the curvature interference limit line are obtained. According to numerical simulation analysis, the influences of the technological crossing angle on worm addendum thickness and the positions of curvature interference limit line on the surfaces of the worm gear and worm are analyzed. Finally, according to its characteristics of the proposed worm, the recommended value range of the technological crossing angle to avoid interference and addendum sharpening is given.

2 Geometry of generating surface of grinding wheel

As shown in Fig. 1, a disk-shaped grinding wheel that can be used to grind the worm blank is rigidly connected to the right-handed coordinate system $\sigma_{\mathrm{d}}\left\{O_{\mathrm{d}};\vec{\boldsymbol{i}}_{\mathrm{d}},\vec{\boldsymbol{j}}_{\mathrm{d}},\vec{\boldsymbol{k}}_{\mathrm{d}}\right\}$. Unit vector $\vec{\boldsymbol{k}}_{\mathrm{d}}$ lies along the central axis of the grinding wheel. The circular arc AB with radius ρ is the profile line of the grinding wheel in the axial section and its location of the origin O_{g} with respect to O_{d} is determined by R_0 and Δ. According to the sphere and circle vector function [18], the vector equation of the generating surface Σ_{d} of the grinding wheel in coordinate system σ_{d} can be represented as

$$\left(\vec{\boldsymbol{r}}_{\mathrm{d}}\right)_{\mathrm{d}}=\overrightarrow{O_{\mathrm{d}}O_{\mathrm{g}}}+\overrightarrow{O_{\mathrm{g}}P}=x_{\mathrm{d}}\vec{\boldsymbol{i}}_{\mathrm{d}}+y_{\mathrm{d}}\vec{\boldsymbol{j}}_{\mathrm{d}}+z_{\mathrm{d}}\vec{\boldsymbol{k}}_{\mathrm{d}} \tag{1}$$

where $x_{\mathrm{d}}=\left(\rho\sin\phi+R_0\right)\cos\theta$, $y_{\mathrm{d}}=\left(\rho\sin\phi+R_0\right)\sin\theta$, $z_{\mathrm{d}}=\rho\cos\phi+\Delta$ and $R_0=R_{\mathrm{g}}-\rho\sin\alpha_{\mathrm{n}}$. Here, θ and ϕ are the curvilinear coordinates of Σ_{d}, α_{n} is profile angle of the grinding wheel at the point Q and R_{g} is the nominal radius of the grinding wheel.

By means of the definition [19], the unit normal vector of Σ_{d} can be expressed as

$$\left(\vec{\boldsymbol{n}}\right)_{\mathrm{d}}=\frac{\dfrac{\partial\left(\vec{\boldsymbol{r}}_{\mathrm{d}}\right)_{\mathrm{d}}}{\partial\theta}\times\dfrac{\partial\left(\vec{\boldsymbol{r}}_{\mathrm{d}}\right)_{\mathrm{d}}}{\partial\phi}}{\left|\dfrac{\partial\left(\vec{\boldsymbol{r}}_{\mathrm{d}}\right)_{\mathrm{d}}}{\partial\theta}\times\dfrac{\partial\left(\vec{\boldsymbol{r}}_{\mathrm{d}}\right)_{\mathrm{d}}}{\partial\phi}\right|}=-\vec{\boldsymbol{m}}_{\mathrm{d}}\left(\theta,\phi\right)=-\sin\phi\cos\theta\vec{\boldsymbol{i}}_{\mathrm{d}}-\sin\phi\sin\theta\vec{\boldsymbol{j}}_{\mathrm{d}}-\cos\phi\vec{\boldsymbol{k}}_{\mathrm{d}} \tag{2}$$

Obviously, its direction is from the space points to the internal entity of the grinding wheel, as shown in Fig. 1.

Besides, based on two principal directions and a unit normal vector, a right-handed movable orthogonal frame $\sigma_{\mathrm{P}}\left\{P;\vec{\boldsymbol{g}}_1,\vec{\boldsymbol{g}}_2,\vec{\boldsymbol{n}}\right\}$ on Σ_{d} at any point P can be formed. From differential geometry [18], the first and second principal directions $\vec{\boldsymbol{g}}_1$ and $\vec{\boldsymbol{g}}_2$ of Σ_{d} can be worked out on the grounds of Eqs. (1) and (2), the results in σ_{d} is

$$(\vec{\boldsymbol{g}}_1)_{\mathrm{d}}=\frac{\dfrac{\partial(\vec{\boldsymbol{r}}_{\mathrm{d}})_{\mathrm{d}}}{\partial\theta}}{\left|\dfrac{\partial(\vec{\boldsymbol{r}}_{\mathrm{d}})_{\mathrm{d}}}{\partial\theta}\right|}=\vec{\boldsymbol{g}}_{\mathrm{d}}\left(\theta\right),\ (\vec{\boldsymbol{g}}_2)_{\mathrm{d}}=\vec{\boldsymbol{n}}_{\mathrm{d}}\times(\vec{\boldsymbol{g}}_1)_{\mathrm{d}}=\vec{\boldsymbol{n}}_{\mathrm{d}}\left(\theta,\phi\right) \tag{3}$$

According to Eq. (3), the first and second principal directions of Σ_{d} are θ-line and ϕ-line directions, respectively. Thus, the parameter curve net of Σ_{d} is also curvature line net.

Accordingly, the two principal curvatures along the principal directions of $(\vec{\boldsymbol{g}}_1)_{\mathrm{d}}$ and $(\vec{\boldsymbol{g}}_2)_{\mathrm{d}}$ can be obtained, respectively, as below

$$k_1=\frac{\sin\phi}{R_0+\rho\sin\phi},\ k_2=\frac{1}{\rho} \tag{4}$$

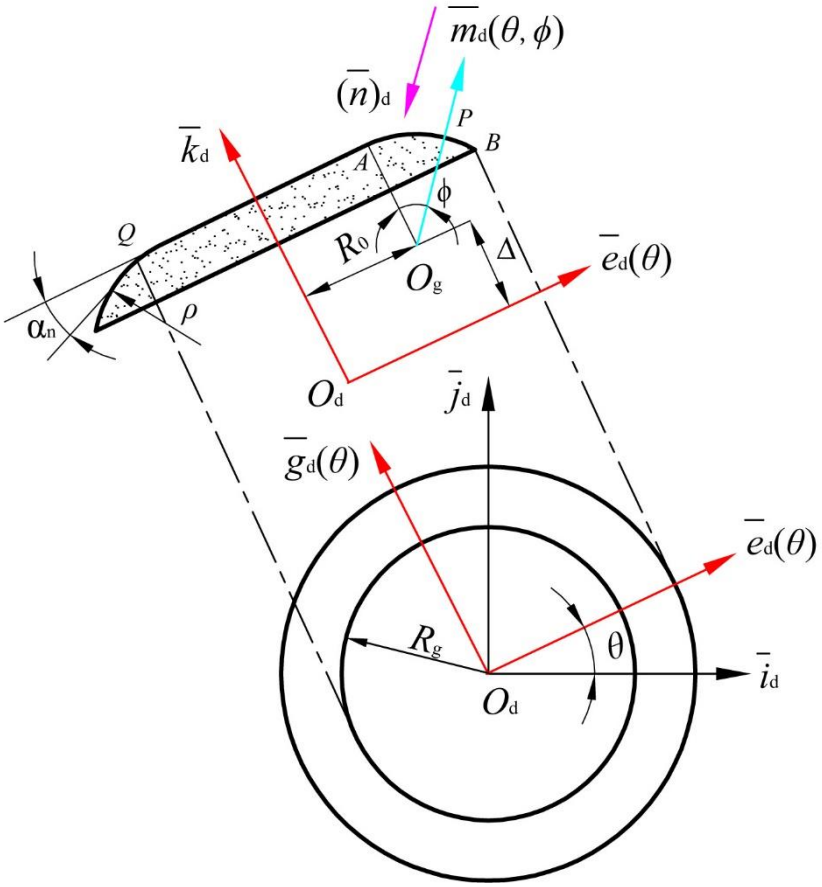

Fig.1 Generating surface of grinding wheel in coordinate system σ_a

3 Mathematical modeling of cutting meshing of Litvin worm

3.1 Relative motion of grinding wheel and worm blank

As shown in Fig. 2(a), during grinding the worm blank, the static coordinate systems σ_d with red dotted line and σ_{o1} are used to indicate the initial positions of the grinding wheel and the worm blank, respectively. The unit vector $\vec{\boldsymbol{k}}_{o1}$ lies along the axis of the worm blank and vectors $\vec{\boldsymbol{i}}_d$ and $\vec{\boldsymbol{i}}_{o1}$ lie along the common perpendicular of the axes between them. In addition, the rotating coordinate system σ_1 is rigidly fixed with the worm blank to denote its current position.

During the generating process, the grinding wheel performs translational motion along the axis $\vec{\boldsymbol{k}}_{o1}$, while the worm blank performs rotational motion around its axis $\vec{\boldsymbol{k}}_{o1}$. At the present position shown in Fig. 2(a), the rotation angle of the worm blank is φ, in the meantime, because the worm is right-handed, the grinding wheel moves $p\varphi$ along the negative direction of the axis $\vec{\boldsymbol{k}}_{o1}$. Herein, p is the screw parameter of the screw motion of the worm.

As shown in Fig. 2(b), at the initial moment, the shortest distance between the axes of the grinding wheel and the worm blank is technological center distance a_d during the cutting engagement, and it can be expressed as $a_d = R_g + d_1/2$. Here, d_1 is the diameter of the worm on its pitch cylinder. Besides, the included angle Σ between the axes of $\vec{\boldsymbol{k}}_d$ and $\vec{\boldsymbol{k}}_{o1}$ is so-called technological crossing angle. The origin O_1 is located at the middle of the worm thread length.

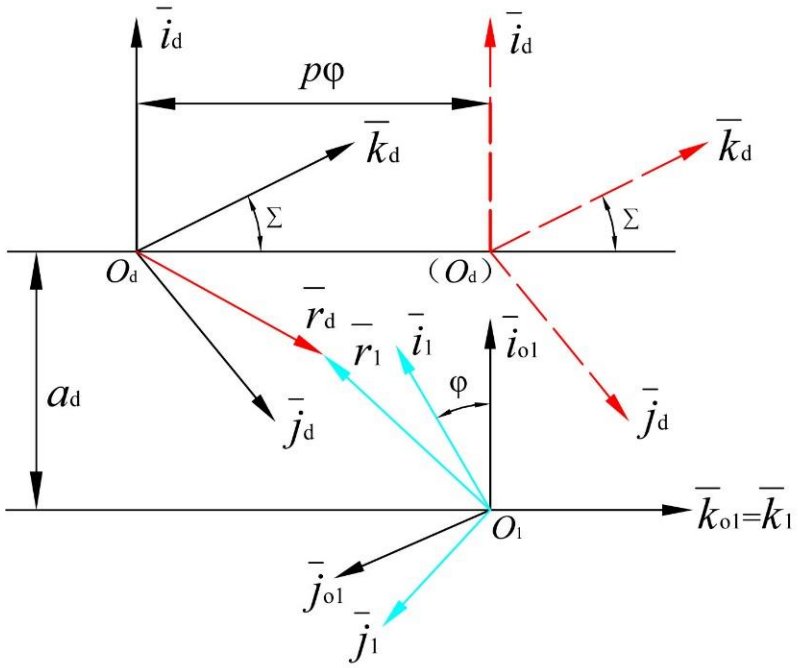

(a) Coordinate system of relative motion between grinding wheel and worm blank

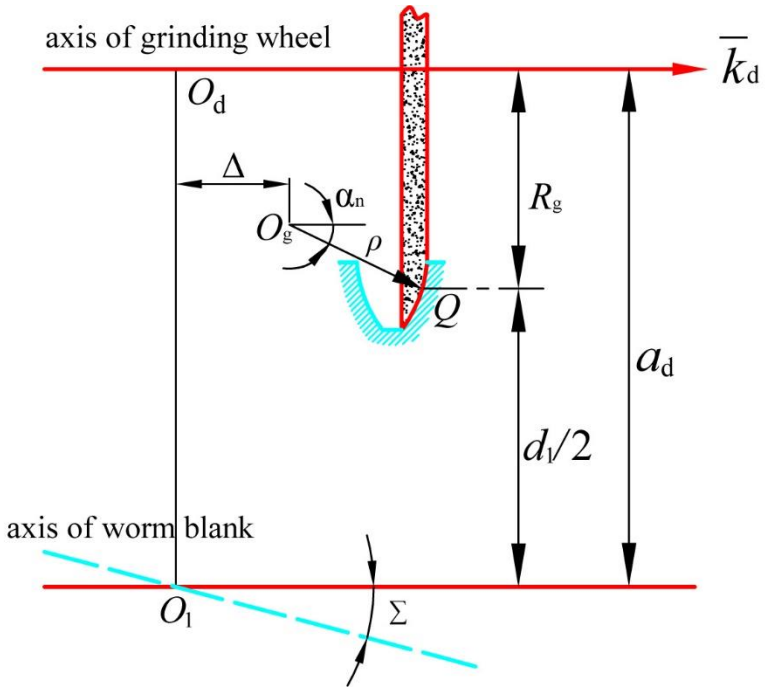

Fig. 2 (b) Position relationship of grinding wheel machining worm blank

Based on the above analysis, it can be learned that the angular velocity of the grinding wheel is zero, that is $\left(\vec{\omega}_d\right)_d = 0$. So, it is reasonable to assume that the angular velocity of the worm blank is 1 rad/s. In this case, the angular velocity vector of the worm blank in coordinate system σ_d can be expressed as $\left(\vec{\omega}_1\right)_d = \sin\Sigma\vec{j}_d + \cos\Sigma\vec{k}_d$. Correspondingly, the relative angular velocity vector between the grinding wheel and the worm blank can be worked out as $\left(\vec{\omega}_{d1}\right)_d = -\sin\Sigma\vec{j}_d - \cos\Sigma\vec{k}_d$. Moreover,

from Fig. 2(a), it can be seen that $\left(\overrightarrow{O_1O_d}\right)_d = a_d\vec{i}_d - p\varphi\sin\Sigma\vec{j}_d - p\varphi\cos\Sigma\vec{k}_d$. Based on this, the relative velocity vector between them can be obtained as below

$$\left(\vec{V}_{d1}\right)_d = \left(\vec{\omega}_{d1}\right)_d \times \left(\vec{r}_d\right)_d - \left(\vec{\omega}_1\right)_d \times \left(\overrightarrow{O_1O_d}\right)_d + \frac{d\left(\overrightarrow{O_1O_d}\right)_d}{d\varphi} = V_{d1}^{(x)}\vec{i}_d + V_{d1}^{(y)}\vec{j}_d + V_{d1}^{(z)}\vec{k}_d \tag{5}$$

where $V_{d1}^{(x)} = y_d\cos\Sigma - z_d\sin\Sigma$, $V_{d1}^{(y)} = -\left(x_d + a_d\right)\cos\Sigma - p\sin\Sigma$, $V_{d1}^{(z)} = \left(x_d + a_d\right)\sin\Sigma - p\cos\Sigma$.

In accordance with the definition [15], the meshing function of the cutting engagement for Litvin worm can be acquired from Eqs. (2) and (5) as

$$\Phi_d\left(\theta,\phi\right) = \left(\vec{n}\right)_d \bullet \left(\vec{V}_{d1}\right)_d = A_d\sin\phi - B_d\cos\phi \tag{6}$$

where $A_d = \left(p\sin\Sigma + a_d\cos\Sigma\right)\sin\theta + \Delta\sin\Sigma\cos\theta$ and $B_d = R_0\sin\Sigma\cos\theta + a_d\sin\Sigma - p\cos\Sigma$. The coefficient A_d of meshing function contains an unknown Δ, and it is the installing parameter Δ of the grinding wheel, which needs to be determined.

In view of the meshing feature of Litvin worm, the instantaneous contact line on the grinding wheel during the cutting engagement is a planar curve. From differential geometry, it can be known that torsion describes the degree of the curve deviating from the plane curve and reflects the degree of curve distortion [18]. Therefore, the necessary and sufficient condition for a curve to be a planar curve is that its torsion is zero. Considering the gear meshing theory and from Eqs. (1) and (6), the equation of the instantaneous contact line can be represented as

$$\left(\vec{r}_d\left(\theta,\phi\right)\right)_d = x_d\left(\theta,\phi\right)\vec{i}_d + y_d\left(\theta,\phi\right)\vec{j}_d + z_d\left(\phi\right)\vec{k}_d,\ \ \Phi_d\left(\theta,\phi\right) = 0 \tag{7}$$

where θ and ϕ are unknown parameters.

From Eq. (7), it can be obtained that the torsion of the instantaneous contact line is $\left[\frac{d\left(\vec{r}_d\right)_d}{d\theta}, \frac{d^2\left(\vec{r}_d\right)_d}{d\theta^2}, \frac{d^3\left(\vec{r}_d\right)_d}{d\theta^3}\right] = 0$. In the process of solving the partial derivative of $\vec{r}_d\left(\theta,\phi\right)$, it can be found that parameters ϕ and θ have no functional relationship. And the value of θ is a constant value $\theta_0 = \pi - \arccos\frac{a_d - p\cot\Sigma}{R_0}$. Based on this, the value range of the technological crossing angle Σ can be obtained as

$$\arctan\frac{p}{a_d} \le \Sigma \le \arctan\frac{p}{d_1/2 + \rho\sin\alpha_n} \tag{8}$$

It is indicated that the value of Σ can be selected in a certain range, which is beneficial to improve the meshing performance of the worm pair. Besides, substituting the expression θ_0 into $A_d = 0$, the parameter value Δ of the installing position of the grinding wheel can be determined, and the outcome is $\Delta = -\tan\theta_0\left(a_d\cot\Sigma + p\right)$.

3.2 Equation of worm helicoid and cutting meshing characteristic parameters

According to the relative motion relationship between the grinding wheel and the worm blank shown in Fig. 2(a), from Eqs. (1) and (2), the equation of the meshing surface Σ_{o1} of the worm and its unit normal vector in σ_{o1} can be represented as

$$\left(\vec{r}_1\right)_{o1} = R\left[\vec{i}_{o1},\Sigma\right]\left(\vec{r}_d\right)_d + \left(\overrightarrow{O_1O_d}\right)_{o1} = \begin{bmatrix} 1 & 0 & 0 \\ 0 & \cos\Sigma & -\sin\Sigma \\ 0 & \sin\Sigma & \cos\Sigma \end{bmatrix}\left(\vec{r}_d\right)_d + \left(\overrightarrow{O_1O_d}\right)_{o1} = x_{o1}\vec{i}_{o1} + y_{o1}\vec{j}_{o1} + z_{o1}\vec{k}_{o1} \tag{9}$$

$$\left(\vec{\boldsymbol{n}}\right)_{\mathrm{o1}}=R\left[\vec{\boldsymbol{i}}_{\mathrm{o1}},\Sigma\right]\left(\vec{\boldsymbol{n}}\right)_{\mathrm{d}}=\begin{bmatrix}1 & 0 & 0\\ 0 & \cos\Sigma & -\sin\Sigma\\ 0 & \sin\Sigma & \cos\Sigma\end{bmatrix}\left(\vec{\boldsymbol{n}}\right)_{\mathrm{d}}=n_{\mathrm{x}}\vec{\boldsymbol{i}}_{\mathrm{o1}}+n_{\mathrm{y}}\vec{\boldsymbol{j}}_{\mathrm{o1}}+n_{\mathrm{z}}\vec{\boldsymbol{k}}_{\mathrm{o1}} \tag{10}$$

where $x_{\mathrm{o1}}=x_{\mathrm{d}}+a_{\mathrm{d}}$, $y_{\mathrm{o1}}=y_{\mathrm{d}}\cos\Sigma-z_{\mathrm{d}}\sin\Sigma$, $z_{\mathrm{o1}}=y_{\mathrm{d}}\sin\Sigma+z_{\mathrm{d}}\cos\Sigma-p\varphi$ and $n_{\mathrm{x}}=-\cos\theta_0\sin\phi$, $n_{\mathrm{y}}=-\cos\Sigma\sin\theta_0\sin\phi+\sin\Sigma\cos\phi$, $n_{\mathrm{z}}=-\sin\Sigma\sin\theta_0\sin\phi-\cos\Sigma\cos\phi$. The symbol $R\left[\vec{\boldsymbol{i}}_{\mathrm{o1}},\Sigma\right]$ denotes the rotation transformation matrices.

Based on Eq. (9) and coordinate transformation, the equation of the worm helicoid Σ_1 can be obtained as

$$\left(\vec{\boldsymbol{r}}_1\right)_1=R\left[\vec{\boldsymbol{k}}_1,-\varphi\right]\left(\vec{\boldsymbol{r}}_1\right)_{\mathrm{o1}}=\begin{bmatrix}\cos\varphi & \sin\varphi & 0\\ -\sin\varphi & \cos\varphi & 0\\ 0 & 0 & 1\end{bmatrix}\left(\vec{\boldsymbol{r}}_1\right)_{\mathrm{o1}}=x_1\vec{\boldsymbol{i}}_1+y_1\vec{\boldsymbol{j}}_1+z_{\mathrm{o1}}\vec{\boldsymbol{k}}_1 \tag{11}$$

where $x_1=x_{\mathrm{o1}}\cos\varphi+y_{\mathrm{o1}}\sin\varphi$, $y_1=-x_{\mathrm{o1}}\sin\varphi+y_{\mathrm{o1}}\cos\varphi$. And here, ϕ and φ are the curvilinear coordinates of Σ_1.

By definition [19], the meshing limit function of the cutting meshing for Litvin worm can be acquired from Eq. (6) as

$$\Phi_{\mathrm{d}\varphi}=\frac{\partial\Phi_{\mathrm{d}}}{\partial\varphi}=0 \tag{12}$$

Due to $\Phi_{\mathrm{d}}=0$, the function $\Phi_{\mathrm{d}\varphi}=0$ is automatically satisfied. Therefore, the meshing limit line and the instantaneous contact line are coincident during the cutting engagement.

On the basis of the meshing theory of gears [19], the coefficients of normal vector $\vec{\boldsymbol{N}}_{\mathrm{d}}$ of the instantaneous contact line during the cutting engagement can be worked out as $\lambda_{\mathrm{d}}=k_1\left(\vec{\boldsymbol{V}}_{\mathrm{d1}}\right)_{\mathrm{d}}\bullet\left(\vec{\boldsymbol{g}}_1\right)_{\mathrm{d}}+\left(\vec{\boldsymbol{\omega}}_{\mathrm{d1}}\right)_{\mathrm{d}}\bullet\left(\vec{\boldsymbol{g}}_2\right)_{\mathrm{d}}=g_{2z}\left(k_1\rho-1\right)-\dfrac{k_1p}{\sin\Sigma\cos\theta_0}$ and $\mu_{\mathrm{d}}=k_2\left(\vec{\boldsymbol{V}}_{\mathrm{d1}}\right)_{\mathrm{d}}\bullet\left(\vec{\boldsymbol{g}}_2\right)_{\mathrm{d}}-\left(\vec{\boldsymbol{\omega}}_{\mathrm{d1}}\right)_{\mathrm{d}}\bullet\left(\vec{\boldsymbol{g}}_1\right)_{\mathrm{d}}=0$, respectively. Therefore, the expression of $\left(\vec{\boldsymbol{N}}_{\mathrm{d}}\right)_{\mathrm{d}}$ in the right-hand orthogonal frame $\sigma_{\mathrm{P}}\left\{P;\vec{\boldsymbol{g}}_1,\vec{\boldsymbol{g}}_2,\vec{\boldsymbol{n}}\right\}$ can be written as

$$\left(\vec{\boldsymbol{N}}_{\mathrm{d}}\right)_{\mathrm{d}}=\lambda_{\mathrm{d}}\left(\vec{\boldsymbol{g}}_1\right)_{\mathrm{d}}+\mu_{\mathrm{d}}\left(\vec{\boldsymbol{g}}_2\right)_{\mathrm{d}}=\lambda_{\mathrm{d}}\left(\vec{\boldsymbol{g}}_1\right)_{\mathrm{d}}=\left[g_{2z}\left(k_1\rho-1\right)-\frac{k_1p}{\sin\Sigma\cos\theta_0}\right]\left(\vec{\boldsymbol{g}}_1\right)_{\mathrm{d}} \tag{13}$$

where $g_{2z}=\sin\Sigma\sin\theta_0\cos\phi-\cos\Sigma\sin\phi$ and its physical meaning will be introduced later. Besides, the expression shows that the normal vector $\vec{\boldsymbol{N}}_{\mathrm{d}}$ of the instantaneous contact line is collinear with the first principal direction $\left(\vec{\boldsymbol{g}}_1\right)_{\mathrm{d}}$ of the generating surface of the grinding wheel.

By definition [19] and Eqs. (3), (5) and (13), the curvature interference limit function of cutting engagement of Litvin worm can be worked out as

$$\Psi_{\mathrm{d}}\left(\phi\right)=\lambda_{\mathrm{d}}\left(\vec{\boldsymbol{V}}_{\mathrm{d1}}\right)_{\mathrm{d}}\bullet\left(\vec{\boldsymbol{g}}_1\right)_{\mathrm{d}}=\left[g_{2z}\left(k_1\rho-1\right)-\frac{k_1p}{\sin\Sigma\cos\theta_0}\right]\left(\rho g_{2z}-\frac{p}{\sin\Sigma\cos\theta_0}\right) \tag{14}$$

On the grounds of the knowledge of differential geometry, the induced normal curvatures of the generating surface Σ_{d} and worm helicoid Σ_1 along the directions of $\left(\vec{\boldsymbol{g}}_1\right)_{\mathrm{d}}$ and $\left(\vec{\boldsymbol{g}}_2\right)_{\mathrm{d}}$, and the induced geodesic torsion $\tau_1^{(\mathrm{d1})}$ along $\left(\vec{\boldsymbol{g}}_1\right)_{\mathrm{d}}$ are: $k_1^{(\mathrm{d1})}=\dfrac{\left[\left(\vec{\boldsymbol{g}}_1\right)_{\mathrm{d}}\bullet\left(\vec{\boldsymbol{N}}_{\mathrm{d}}\right)_{\mathrm{d}}\right]^2}{\Psi_{\mathrm{d}}}=\dfrac{\left[\left(\vec{\boldsymbol{g}}_1\right)_{\mathrm{d}}\bullet\lambda_{\mathrm{d}}\left(\vec{\boldsymbol{g}}_1\right)_{\mathrm{d}}\right]^2}{\Psi_{\mathrm{d}}}=\dfrac{\lambda_{\mathrm{d}}^2}{\Psi_{\mathrm{d}}}$,

$k_2^{(\mathrm{d}1)}=\dfrac{\left[(\vec{\boldsymbol{g}}_2)_{\mathrm{d}}\bullet(\vec{\boldsymbol{N}}_{\mathrm{d}})_{\mathrm{d}}\right]^2}{\Psi_{\mathrm{d}}}=\dfrac{\left[(\vec{\boldsymbol{g}}_2)_{\mathrm{d}}\bullet\lambda_{\mathrm{d}}(\vec{\boldsymbol{g}}_1)_{\mathrm{d}}\right]^2}{\Psi_{\mathrm{d}}}=0$ and $\tau_1^{(\mathrm{d}1)}=\dfrac{\lambda_{\mathrm{d}}\mu_{\mathrm{d}}}{\Psi_{\mathrm{d}}}=0$, respectively. Therefore, two normal curvatures $k_1^{(1)}$ and $k_2^{(1)}$ in the worm helicoid along the $(\vec{\boldsymbol{g}}_1)_{\mathrm{d}}$ and $(\vec{\boldsymbol{g}}_2)_{\mathrm{d}}$, respectively, and the geodesic torsion $\tau_1^{(1)}$ along $(\vec{\boldsymbol{g}}_1)_{\mathrm{d}}$ can be obtained as follows

$$k_1^{(1)}=k_1-k_1^{(\mathrm{d}1)}=\frac{g_{2z}\sin\Sigma\cos\theta_0}{D_k},\quad k_2^{(1)}=k_2-k_2^{(\mathrm{d}1)}=\frac{1}{\rho},\quad \tau_1^{(1)}=\tau_1^{(\mathrm{d})}=0 \tag{15}$$

where $D_k=\rho g_{2z}\sin\Sigma\cos\theta_0-p$. Here, $\tau_1^{(1)}=0$ indicates that the direction it is in is the principal direction of the worm helicoid.

4 Mathematical modeling of working meshing of worm pair

4.1 Relative motion of worm pair and equation of tooth surface

The relative motion relationship of the worm and the worm gear is shown in Fig. 3. Similar to the coordinate system $\sigma_{\mathrm{o}1}$ and σ_1 of the worm, the static coordinate system $\sigma_{\mathrm{o}2}\{O_2;\vec{\boldsymbol{i}}_{\mathrm{o}2},\vec{\boldsymbol{j}}_{\mathrm{o}2},\vec{\boldsymbol{k}}_{\mathrm{o}2}\}$ is used to indicate the initial position of the worm gear and the rotating coordinate system $\sigma_2\{O_2;\vec{\boldsymbol{i}}_2,\vec{\boldsymbol{j}}_2,\vec{\boldsymbol{k}}_2\}$ is rigidly connect to the worm gear to express its present position. The origin O_2 is situated in the middle of the tooth width of the worm gear. Unit vector $\vec{\boldsymbol{k}}_{\mathrm{o}2}$ is consistent with the axis of the worm gear. In this paper, the axes of the worm and the worm gear are orthogonal and unit vectors $\vec{\boldsymbol{i}}_{\mathrm{o}1}$ and $\vec{\boldsymbol{i}}_{\mathrm{o}2}$ are collinear along the direction of the common perpendicular between the axes $\vec{\boldsymbol{k}}_{\mathrm{o}1}$ and $\vec{\boldsymbol{k}}_{\mathrm{o}2}$. The distance between the common perpendicular of the worm pair is $|\overrightarrow{O_2O_1}|=a$. Herein, the symbol a denotes the center distance of the worm pair.

In the process of meshing of the worm pair, the worm rotates the angle φ_1 around the axis $\vec{\boldsymbol{k}}_{\mathrm{o}1}$ at an angle velocity $\vec{\boldsymbol{\omega}}_1$ shown in Fig. 3 and the worm gear rotates the angle φ_2 around the axis $\vec{\boldsymbol{k}}_{\mathrm{o}2}$ at an angle velocity $\vec{\boldsymbol{\omega}}_2$. Here, the relationship between the rotation angles φ_1 and φ_2 is $\varphi_2=\varphi_1/i_{12}$, and i_{12} denotes the transmission ratio of the worm pair.

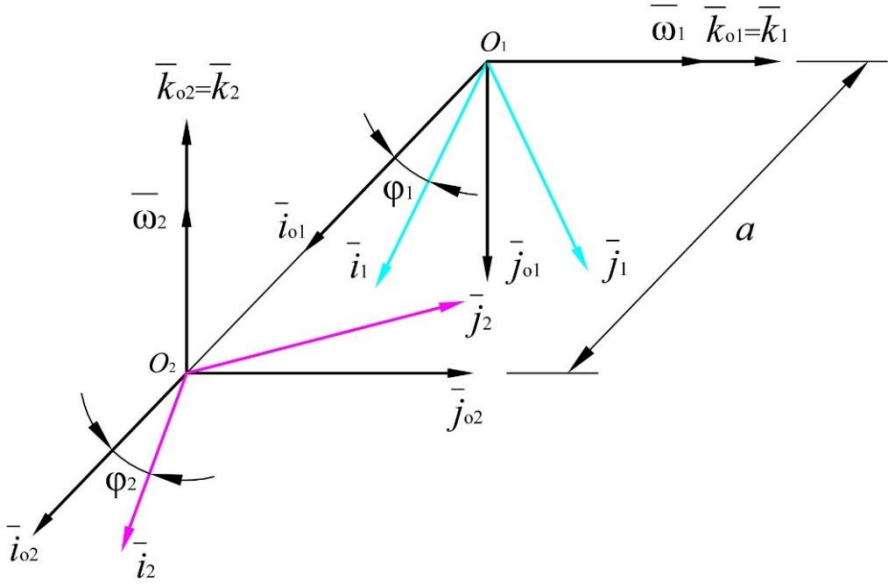

Fig. 3 Coordinate system for studying meshing of worm pair

Based on the above analysis, when the worm rotates around its axis $\vec{\boldsymbol{k}}_{o1}$, a surface family $\{\Sigma_1\}$ will come into being from its helicoid in coordinate system σ_{o1}. By means of Eqs. (9) and (10), the equation of $\{\Sigma_1\}$ and its unit normal vector can be represented as

$$\left(\vec{\boldsymbol{r}}_1^{\,*}\right)_{o1}=\begin{bmatrix}\cos\left(\varphi_1-\varphi\right) & -\sin\left(\varphi_1-\varphi\right) & 0\\ \sin\left(\varphi_1-\varphi\right) & \cos\left(\varphi_1-\varphi\right) & 0\\ 0 & 0 & 1\end{bmatrix}\left(\vec{\boldsymbol{r}}_1\right)_{o1}=x_{o1}^{*}\vec{\boldsymbol{i}}_{o1}+y_{o1}^{*}\vec{\boldsymbol{j}}_{o1}+z_{o1}\vec{\boldsymbol{k}}_{o1} \tag{16}$$

$$\left(\vec{\boldsymbol{n}}^{*}\right)_{o1}=\begin{bmatrix}\cos\left(\varphi_1-\varphi\right) & -\sin\left(\varphi_1-\varphi\right) & 0\\ \sin\left(\varphi_1-\varphi\right) & \cos\left(\varphi_1-\varphi\right) & 0\\ 0 & 0 & 1\end{bmatrix}\left(\vec{\boldsymbol{n}}\right)_{o1}=n_{ox}\vec{\boldsymbol{i}}_{o1}+n_{oy}\vec{\boldsymbol{j}}_{o1}+n_{z}\vec{\boldsymbol{k}}_{o1} \tag{17}$$

where $x_{o1}^{*}=x_{o1}\cos\left(\varphi_1-\varphi\right)-y_{o1}\sin\left(\varphi_1-\varphi\right)$, $y_{o1}^{*}=x_{o1}\sin\left(\varphi_1-\varphi\right)+y_{o1}\cos\left(\varphi_1-\varphi\right)$ and $n_{ox}=n_{x}\cos\left(\varphi_1-\varphi\right)-n_{y}\sin\left(\varphi_1-\varphi\right)$, $n_{oy}=n_{x}\sin\left(\varphi_1-\varphi\right)+n_{y}\cos\left(\varphi_1-\varphi\right)$.

Without loss of generality, it is possible to suppose that the worm rotates around its axis with an angle velocity $\left|\vec{\boldsymbol{\omega}}_1\right|=1\,\mathrm{rad/s}$, and the angle velocity of the worm gear is $\left|\vec{\boldsymbol{\omega}}_2\right|=1/i_{12}\ \mathrm{rad/s}$ on the basis of their transmission ratio. According to the relative motion relationship shown in Fig. 3, the angle velocity vectors of the worm and the worm gear are $\left(\vec{\boldsymbol{\omega}}_1\right)_{o1}=\vec{\boldsymbol{k}}_{o1}$ and $\left(\vec{\boldsymbol{\omega}}_2\right)_{o1}=-\dfrac{1}{i_{12}}\vec{\boldsymbol{j}}_{o1}$ in σ_{o1}, respectively. Hence, the relative angle velocity vector between them in σ_{o1} is

$$\left(\vec{\boldsymbol{\omega}}_{12}\right)_{o1}=\left(\vec{\boldsymbol{\omega}}_1\right)_{o1}-\left(\vec{\boldsymbol{\omega}}_2\right)_{o1}=\frac{1}{i_{12}}\vec{\boldsymbol{j}}_{o1}+\vec{\boldsymbol{k}}_{o1} \tag{18}$$

Due to $\left(\overrightarrow{O_2O_1}\right)_{o1}=-a\vec{\boldsymbol{i}}_{o1}$, from Eqs. (16) and (18), the relative velocity vector between the worm and the worm gear can be figured out in σ_{o1}, the result is

$$\left(\vec{\boldsymbol{V}}_{12}\right)_{o1}=\left(\vec{\boldsymbol{\omega}}_{12}\right)_{o1}\times\left(\vec{\boldsymbol{r}}_1^{\,*}\right)_{o1}-\left(\vec{\boldsymbol{\omega}}_2\right)_{o1}\times\left(\overrightarrow{O_2O_1}\right)_{o1}=\frac{1}{i_{12}}\left(z_{o1}-i_{12}y_{o1}^{*}\right)\vec{\boldsymbol{i}}_{o1}+x_{o1}^{*}\vec{\boldsymbol{j}}_{o1}-\frac{1}{i_{12}}\left(x_{o1}^{*}-a\right)\vec{\boldsymbol{k}}_{o1} \tag{19}$$

In virtue of the Eqs. (17) and (19), the meshing function of working engagement for Litvin worm pair can be obtained as

$$\Phi=\Phi\left(\phi,\varphi,\varphi_1\right)=\left(\vec{\boldsymbol{n}}^{*}\right)_{o1}\bullet\left(\vec{\boldsymbol{V}}_{12}\right)_{o1}=\frac{1}{i_{12}}\left[A\sin\left(\varphi_1-\varphi\right)+B\cos\left(\varphi_1-\varphi\right)+C\right] \tag{20}$$

where $A=n_{z}y_{o1}-n_{y}z_{o1}$, $B=n_{x}z_{o1}-n_{z}x_{o1}$, $C=\left(a-i_{12}p\right)n_{z}$.

With the aid of Eqs. (16) and (20), the equation of the tooth surface of the worm gear can be acquired as below

$$\begin{cases}\left(\vec{\boldsymbol{r}}_2\right)_2=R\left[\vec{\boldsymbol{k}}_2,-\dfrac{\varphi_1}{i_{12}}\right]\left\{R\left[\vec{\boldsymbol{i}}_{o2},-90^{\circ}\right]\left(\vec{\boldsymbol{r}}_1^{\,*}\right)_{o1}+\left(\overrightarrow{O_2O_1}\right)_{o2}\right\}=x_2\vec{\boldsymbol{i}}_2+y_2\vec{\boldsymbol{j}}_2+z_2\vec{\boldsymbol{k}}_2\\ \Phi\left(\phi,\varphi,\varphi_1\right)=0\end{cases} \tag{21}$$

where $x_2=\left(x_{o1}^{*}-a\right)\cos\dfrac{\varphi_1}{i_{12}}+z_{o1}\sin\dfrac{\varphi_1}{i_{12}}$, $y_2=-\left(x_{o1}^{*}-a\right)\sin\dfrac{\varphi_1}{i_{12}}+z_{o1}\cos\dfrac{\varphi_1}{i_{12}}$ and $z_2=-y_{o1}^{*}$. Herein,

$$R\left[\vec{\boldsymbol{k}}_2,-\frac{\varphi_1}{i_{12}}\right]=\begin{bmatrix}\cos\dfrac{\varphi_1}{i_{12}} & \sin\dfrac{\varphi_1}{i_{12}} & 0\\ -\sin\dfrac{\varphi_1}{i_{12}} & \cos\dfrac{\varphi_1}{i_{12}} & 0\\ 0 & 0 & 1\end{bmatrix} \text{ and } R\left[\vec{\boldsymbol{i}}_{o2},-90^\circ\right]=\begin{bmatrix}1 & 0 & 0\\ 0 & 0 & 1\\ 0 & -1 & 0\end{bmatrix}.$$

4.2 Function of interference limit line and its characteristics parameters

From Eq. (20), the meshing limit function of working engagement for Litvin worm pair can be obtained as

$$\Phi_{\varphi_1}=\frac{\partial\Phi}{\partial\varphi_1}=\frac{1}{i_{12}}\left[A\cos\left(\varphi_1-\varphi\right)-B\sin\left(\varphi_1-\varphi\right)\right] \tag{22}$$

In accordance with Eq. (3), the two base vectors $\vec{\boldsymbol{g}}_1^{(1)}$ and $\vec{\boldsymbol{g}}_2^{(1)}$ in coordinate system σ_{o1} can be represented as

$$\begin{aligned}\vec{\boldsymbol{g}}_1^{(1)}&=R\left[\vec{\boldsymbol{k}}_{o1},\varphi_1-\varphi\right]R\left[\vec{\boldsymbol{i}}_{o1},\Sigma\right]\left(\vec{\boldsymbol{g}}_1\right)_d=g_{1x}\vec{\boldsymbol{i}}_{o1}+g_{1y}\vec{\boldsymbol{j}}_{o1}+g_{1z}\vec{\boldsymbol{k}}_{o1}\\ \vec{\boldsymbol{g}}_2^{(1)}&=R\left[\vec{\boldsymbol{k}}_{o1},\varphi_1-\varphi\right]R\left[\vec{\boldsymbol{i}}_{o1},\Sigma\right]\left(\vec{\boldsymbol{g}}_2\right)_d=g_{2x}\vec{\boldsymbol{i}}_{o1}+g_{2y}\vec{\boldsymbol{j}}_{o1}+g_{2z}\vec{\boldsymbol{k}}_{o1}\end{aligned} \tag{23}$$

where $g_{1x}=-\sin\theta_0\cos\left(\varphi_1-\varphi\right)-\cos\Sigma\cos\theta_0\sin\left(\varphi_1-\varphi\right)$,

$g_{1y}=-\sin\theta_0\sin\left(\varphi_1-\varphi\right)+\cos\Sigma\cos\theta_0\cos\left(\varphi_1-\varphi\right)$, $g_{1z}=\sin\Sigma\cos\theta_0$,

$g_{2x}=\cos\theta_0\cos\phi\cos\left(\varphi_1-\varphi\right)-\left(\cos\Sigma\sin\theta_0\cos\phi+\sin\Sigma\sin\phi\right)\sin\left(\varphi_1-\varphi\right)$,

$g_{2y}=\cos\theta_0\cos\phi\sin\left(\varphi_1-\varphi\right)+\left(\cos\Sigma\sin\theta_0\cos\phi+\sin\Sigma\sin\phi\right)\cos\left(\varphi_1-\varphi\right)$,

$g_{2z}=\sin\Sigma\sin\theta_0\cos\phi-\cos\Sigma\sin\phi$. Here, $\vec{\boldsymbol{g}}_1^{(1)}$ and $\vec{\boldsymbol{g}}_2^{(1)}$ are the two principal directions of the worm helicoid.

The normal vector $\vec{\boldsymbol{N}}$ of the instantaneous contact line of the working engagement can be expressed by the base vectors $\vec{\boldsymbol{g}}_1^{(1)}$ and $\vec{\boldsymbol{g}}_2^{(1)}$ in σ_{o1}, the outcome is

$$\left(\vec{\boldsymbol{N}}\right)_{o1}=N_1\vec{\boldsymbol{g}}_1^{(1)}+N_2\vec{\boldsymbol{g}}_2^{(1)} \tag{24}$$

Based on Eqs. (15), (18), (19) and (23), the coefficients N_1 and N_2 of unit normal vector of the instantaneous contact line can be acquired as

$$N_1=k_1^{(1)}\left(\vec{\boldsymbol{V}}_{12}\right)_{o1}\bullet\vec{\boldsymbol{g}}_1^{(1)}+\left(\vec{\boldsymbol{\omega}}_{12}\right)_{o1}\bullet\vec{\boldsymbol{g}}_2^{(1)},\quad N_2=k_2^{(1)}\left(\vec{\boldsymbol{V}}_{12}\right)_{o1}\bullet\vec{\boldsymbol{g}}_2^{(1)}-\left(\vec{\boldsymbol{\omega}}_{12}\right)_{o1}\bullet\vec{\boldsymbol{g}}_1^{(1)} \tag{25}$$

where $\left(\vec{\boldsymbol{V}}_{12}\right)_{o1}\bullet\vec{\boldsymbol{g}}_1^{(1)}=\dfrac{g_{1x}}{i_{12}}\left(z_{o1}-i_{12}y_{o1}^*\right)+g_{1y}x_{o1}^*+\dfrac{\sin\Sigma\cos\theta_0}{i_{12}}\left(a-x_{o1}^*\right)$, $\left(\vec{\boldsymbol{\omega}}_{12}\right)_{o1}\bullet\vec{\boldsymbol{g}}_2^{(1)}=\dfrac{g_{2y}}{i_{12}}+g_{2z}$,

$\left(\vec{\boldsymbol{V}}_{12}\right)_{o1}\bullet\vec{\boldsymbol{g}}_2^{(1)}=\dfrac{g_{2x}}{i_{12}}\left(z_{o1}-i_{12}y_{o1}^*\right)+g_{2y}x_{o1}^*+\dfrac{g_{2z}}{i_{12}}\left(a-x_{o1}^*\right)$, and $\left(\vec{\boldsymbol{\omega}}_{12}\right)_{o1}\bullet\vec{\boldsymbol{g}}_1^{(1)}=\dfrac{g_{1y}}{i_{12}}+\sin\Sigma\cos\theta_0$.

From Eqs. (22) and (25), the curvature interference limit function of the working engagement for Litvin worm pair can be determined as below

$$\Psi=N_1\left(\vec{\boldsymbol{V}}_{12}\right)_{o1}\bullet\vec{\boldsymbol{g}}_1^{(1)}+N_2\left(\vec{\boldsymbol{V}}_{12}\right)_{o1}\bullet\vec{\boldsymbol{g}}_2^{(1)}+\Phi_{\varphi1} \tag{26}$$

By projecting the vector $\left(\vec{\boldsymbol{V}}_{12}\right)_{o1}$ into the principal frame $\left\{\vec{\boldsymbol{g}}_1^{(1)},\vec{\boldsymbol{g}}_2^{(1)},\left(\vec{\boldsymbol{n}}^*\right)_{o1}\right\}$ of worm helicoid, the vector $\left(\vec{\boldsymbol{V}}_{12}\right)_{o1}$ can be expressed as $\left(\vec{\boldsymbol{V}}_{12}\right)_{o1}=\left[\left(\vec{\boldsymbol{V}}_{12}\right)_{o1}\bullet\vec{\boldsymbol{g}}_1^{(1)}\right]\vec{\boldsymbol{g}}_1^{(1)}+\left[\left(\vec{\boldsymbol{V}}_{12}\right)_{o1}\bullet\vec{\boldsymbol{g}}_2^{(1)}\right]\vec{\boldsymbol{g}}_2^{(1)}$. Therefore, the

relationship among $\left(\vec{\boldsymbol{V}}_{12}\right)_{o1}\bullet\left(\vec{\boldsymbol{V}}_{12}\right)_{o1}$, $\left[\left(\vec{\boldsymbol{V}}_{12}\right)_{o1}\bullet\vec{\boldsymbol{g}}_1^{(1)}\right]^2$ and $\left[\left(\vec{\boldsymbol{V}}_{12}\right)_{o1}\bullet\vec{\boldsymbol{g}}_2^{(1)}\right]^2$ can be expressed as below

$$\left(\vec{\boldsymbol{V}}_{12}\right)_{o1}\bullet\left(\vec{\boldsymbol{V}}_{12}\right)_{o1}=\left[\left(\vec{\boldsymbol{V}}_{12}\right)_{o1}\bullet\vec{\boldsymbol{g}}_1^{(1)}\right]^2+\left[\left(\vec{\boldsymbol{V}}_{12}\right)_{o1}\bullet\vec{\boldsymbol{g}}_2^{(1)}\right]^2 \tag{27}$$

By means of Eqs. (25), (27) and the expression $\Phi_{\varphi_1}=\frac{1}{i_{12}}\left(y_{o1}^{*}n_z-z_{o1}n_{oy}\right)$ of the meshing limit function, the curvature interference limit function, Ψ, can be written as

$$\begin{aligned}\Psi=&\left(k_1^{(1)}-k_2^{(1)}\right)\left[\left(\vec{\boldsymbol{V}}_{12}\right)_{o1}\bullet\vec{\boldsymbol{g}}_1^{(1)}\right]^2+k_2^{(1)}\left(\vec{\boldsymbol{V}}_{12}\right)_{o1}^2+\left(\frac{1}{i_{12}^2}n_z-\frac{1}{i_{12}}n_{oy}\right)z_{o1}\\&-\frac{y_{o1}^{*}}{i_{12}^2}n_{oy}-\frac{a}{i_{12}^2}n_{ox}+\left(\frac{1}{i_{12}^2}+1\right)\left(n_x x_{o1}+n_y y_{o1}\right)\end{aligned} \tag{28}$$

5 Relationship between worm addendum thickness and technological crossing angle

In order to reveal the general rule of worm addendum sharpening, it is necessary to calculate the tooth profile in the axial section of the worm accurately and obtain its addendum thickness.

5.1 Design of main parameters

In the design of parameters, considering the problem of the worm addendum sharpening, the worm addendum height is selected as $0.8m$. Here, m is module. Besides, the technological crossing angle is selected as the maximum value $9.79°$ based on Eq. (8). The main design parameters of the worm pair and the technological parameters of the worm during the cutting engagement are provided in Tables 1 and 2.

Table 1. Main design parameters of worm pair

Nomenclature	Symbol and formula	Value
Center distance	a	200mm
Transmission ratio	i_{12}	20
Numbers of worm thread	Z_1	2
Pitch circle diameter of worm	d_1	64mm
Teeth number of worm gear	$Z_2=i_{12}Z_1$	40
Module	$m\approx(1.4\sim1.7)a/Z_2$	8mm
Modification coefficient of worm gear	$\zeta=a/m-(d_1/m+Z_2)/2$	1
Height of addendum of worm	$h_{a1}=0.8m$	6.4mm
Tip circle radius of worm	$r_{a1}=d_1/2+0.8m$	38.4mm
Root circle radius of worm	$r_{f1}=d_1/2-1.16m$	21.12mm
Tooth thickness of the worm on its indexing circle	$s_1=0.4\pi m$	10.0531mm
Guide angle of worm indexing cylinder	$\gamma=\arctan mZ_1/d_1$	14.0362°
Tooth width of worm	$L_w\approx3m\sqrt{Z_2+1}$	153.675mm
Throat circle radius of worm gear	$r_{a2}=(Z_2/2+\zeta+1)m$	176mm
Root circus radius of worm gear	$r_{f2}=(Z_2/2+\zeta-1.16)m$	158.72mm
Outer circle radius of worm gear	$r_{e2}=(Z_2/2+\zeta+1.4)m$	179.2mm

Table 2. Processing parameters of worm

Nomenclature	Symbol and formula	Value
Nominal radius of grinding wheel	R_g	120mm
Operating center distance	$a_d = R_g + d_1/2$	152mm
Shape angle of grinding wheel	α_n	21°
Radius of arc profile	$\rho = 5m$	40mm
Technological crossing angle	Σ	9.79°
Parameter of grinding wheel	$\theta_0 = \pi - \arccos\dfrac{a_d - p\cot\Sigma}{R_0}$	178.6654°
Installing position parameter	$\Delta = -\tan\theta_0\left(a_d\cot\Sigma + p\right)$	20.6807mm

5.2 Tooth profile geometry of worm and calculation of worm addendum thickness

During grinding the worm blank, the rotating coordinate system $\sigma_1\left\{O_1;\vec{i}_1,\vec{j}_1,\vec{k}_1\right\}$ connected to the worm blank, and unit vectors $\vec{i}_1$ and $\vec{j}_1$ on the axial section of the worm are not located in the horizontal and vertical positions. For observing the worm tooth profile conveniently, it is essential to rotate the coordinate system σ_1 around the axis $\vec{k}_1$ with an angle η to get a new coordinate system $\sigma_t\left\{O_1;\vec{i}_t,\vec{j}_t,\vec{k}_t\right\}$. As shown in Fig. 4, in coordinate system σ_t, the axes $\vec{i}_t$ and $\vec{j}_t$ are situated in the horizontal and vertical positions, respectively. In this case, by virtue of Eq. (11) and coordinate transformation, the equation of the tooth profile of the worm can be represented in σ_t as

$$\begin{cases} y_t\left(\phi,\varphi,\eta\right)=0 \\ \left(\vec{r}_1\right)_t = R\left[\vec{k}_1,\eta-\varphi\right]\left(\vec{r}_1\right)_{o1} = x_t\vec{i}_t + z_t\vec{k}_t \end{cases} \tag{29}$$

where $x_t = x_{o1}\cos\left(\eta-\varphi\right) - y_{o1}\sin\left(\eta-\varphi\right)$, $y_t = x_{o1}\sin\left(\eta-\varphi\right) + y_{o1}\cos\left(\eta-\varphi\right)$, $z_t = z_{o1}$.

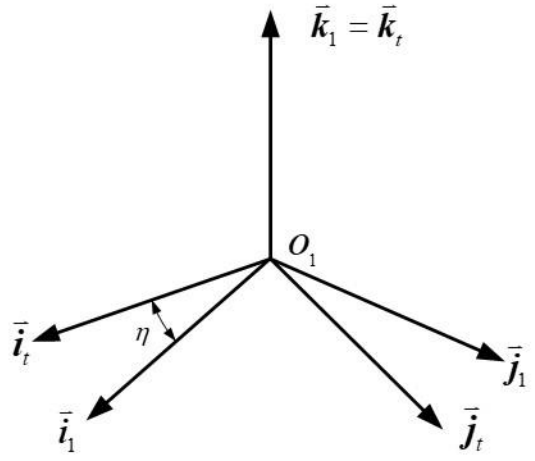

Fig. 4 Rotational coordinate system of tooth profile

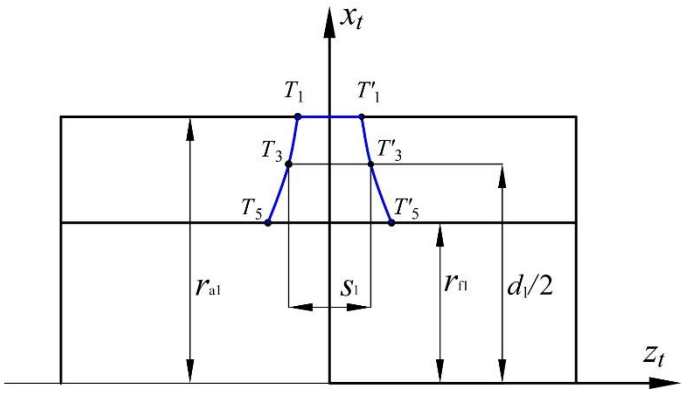

Fig. 5 Worm tooth profile on the axial section

The tooth profile of the worm on the axial section $\left\{O_1;\vec{i}_t,\vec{k}_t\right\}$ is shown in Fig. 5, the coordinate axes x_t and z_t are the components of unit vectors $\vec{i}_t$ and $\vec{k}_t$ respectively. In addition, the tooth profile is symmetrical about x_t axis. In the light of Fig. 5, the tooth profile of the worm can be determined by taking the following steps: firstly, the coordinates of three key points from T_1 to T_5

on the tooth profile in σ_t are obtained. And then three points are fitted into a curve by interpolation method. Finally, according to the symmetry of the tooth profile, its complete shape on the axial section of the worm can be acquired. It can be seen from above that the most important step is the first. Now, the solving method of the key points will be introduced.

The first point to be solved is T_3. Because the point T_3 located on the indexing circle of the worm, the distance from T_3 to T_3' is the tooth thickness s_1 of the worm on its indexing circle. Therefore, its abscissa and ordinate are $z_t = -s_1/2$ and $x_t = d_1/2$, respectively. Based on the coordinate relationship, the following equations can be obtained at the point T_3 as

$$x_t(\phi,\varphi,\eta) = d_1/2,\quad y_t(\phi,\varphi,\eta) = 0,\quad z_t(\phi,\varphi) = -s_1/2 \tag{30}$$

There are three unknowns ϕ, φ and η in Eq. (30).

From the first two expressions of Eq. (30) and expressions of coordinate component of Eq. (1), a nonlinear equation with one variable ϕ can be acquired as

$$f_{T_3}(\phi) = \left[(\rho\sin\phi + R_0)\cos\theta_0 + a_\mathrm{d}\right]^2 + \left[(\rho\sin\phi + R_0)\sin\theta_0\cos\Sigma - (\rho\cos\phi + \Delta)\sin\Sigma\right]^2 - \frac{d_1^2}{4} = 0 \tag{31}$$

With the aid of the third expression of Eq. (30), it is possible to have

$$\varphi(\phi) = \frac{(\rho\sin\phi + R_0)\sin\theta_0\sin\Sigma + (\rho\cos\phi + \Delta)\cos\Sigma + s_1/2}{p} \tag{32}$$

which indicates that parameter φ is a single parameter function regarding ϕ.

Based on the first two expressions of Eq. (30), the expressions about $\eta - \varphi$ can be obtained as

$$\sin(\eta-\varphi) = -\frac{y_{o1}d_1}{2\left(x_{o1}^2 + y_{o1}^2\right)},\quad \cos(\eta-\varphi) = \frac{x_{o1}d_1}{2\left(x_{o1}^2 + y_{o1}^2\right)} \tag{33}$$

From Eqs. (31)-(33), the value of ϕ is obtained, the parameter values of φ and η can be solved accordingly. Thus, the point T_3 can be determined by means of given parameters in Tables 1 and 2, and its parameter values are listed in Table 3.

The point T_1 is located on the worm addendum, as shown in Fig.5. Thus, its ordinate x_t is r_{a1}, where r_{a1} is the radius of the worm on its addendum circle. Besides, the value of η has been worked out in the process of solving the point T_3. Based on this, the expressions of the coordinate component of the point T_1 can be written as

$$x_t(\phi,\varphi) = r_{a1},\quad y_t(\phi,\varphi) = 0 \tag{34}$$

There are two unknowns ϕ and φ in Eq. (34).

From Eq. (34) and expressions of coordinate component of Eq. (1), a nonlinear equation with one variable ϕ can be acquired as

$$f_{T_3}(\phi) = \left[(\rho\sin\phi + R_0)\cos\theta_0 + a_\mathrm{d}\right]^2 + \left[(\rho\sin\phi + R_0)\sin\theta_0\cos\Sigma - (\rho\cos\phi + \Delta)\sin\Sigma\right]^2 - r_{a1}^2 = 0 \tag{35}$$

Eq. (34) leads up to

$$\sin(\eta-\varphi) = -\frac{y_{o1}r_{a1}}{x_{o1}^2 + y_{o1}^2},\quad \cos(\eta-\varphi) = \frac{x_{o1}r_{a1}}{x_{o1}^2 + y_{o1}^2} \tag{36}$$

It is similar to solving the point T_3, and its parameter values are provided in Table 3.

In the process of solving the point T_5, we only need to replace r_{a1} with r_{f1} in Eqs. (34)- (36) and other procedures are the same as solving the point T_1. Thus, the unnecessary details will not be given again. In addition, in order to increase the accuracy of the worm profile, the points T_2 and T_4

are added, and their ordinates are $(r_{a1}-d_1/2)/2+d_1/2$ and $(d_1/2-r_{f1})/2+r_{f1}$, respectively. Their parameter values are also supplied in Table 3. Eventually, the image of the tooth profile in the axial section of the worm is described by interpolation method, as shown in Fig. 6. In this image, the worm addendum thickness is $s_a=-2z_{o1}^{(a)}=6.51\,\text{mm}$, $z_{o1}^{(a)}$ is the abscissa of the point T_1.

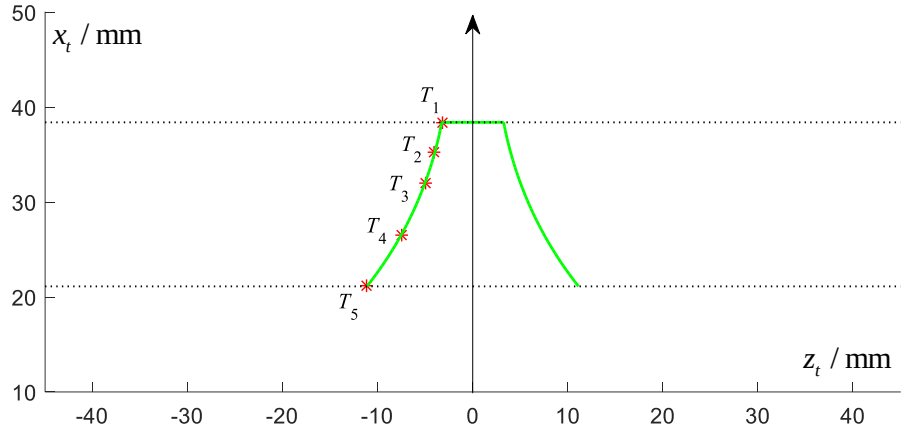

Fig. 6 Tooth profile on axial section of worm

Table 3 Parameter values of key points on tooth profile curve

$\eta=459.3632°$				
Tooth shape point	ϕ / °	φ / °	x_t / mm	z_t / mm
T_1	12.5796	448.0473	38.4	-3.2562
T_2	17.3593	447.3712	35.2	-3.9981
T_3	22.2591	446.6492	32	-5.0265
T_4	31.0049	445.3028	26.56	-7.5114
T_5	40.5865	443.8074	21.12	-11.1323

According to the above analysis, the calculation formula of the worm addendum thickness can be summarized as follows

$$s_a(\phi,\varphi)=-2z_{o1}^{(a)}=2\left[p\varphi-(\rho\sin\phi+R_0)\sin\theta_0\sin\Sigma-(\rho\cos\phi+\Delta)\cos\Sigma\right] \tag{37}$$

There are two unknowns ϕ and φ in this formula, both of which are the parameters of the worm addendum. Before calculating these two unknowns, the rotating angle η of the worm around its axis needs to be determined first by means of Eqs. (31)-(33), and then the values ϕ and φ are obtained from Eqs. (35) and (36). Based on this, the worm addendum thickness is gotten.

5.3 Determination of minimum value of technological crossing angle

In section 3.1, according to the fact that the instantaneous contact line is a planar curve on the grinding wheel during the cutting engagement, the value range of the technological crossing angle Σ is determined. Nevertheless, in the process of actual production and manufacture, if the value of Σ is selected too small, it will cause the worm addendum sharpening, which causes the bearing capacity of the worm reduced and even can't work normally. In this section, the minimum value of Σ satisfying the worm addendum thickness will be obtained.

According to Eq. (8) and the parameters listed in Tables 1 and 2, the value range of Σ can be calculated as $[1.78°,9.79°]$. In order to directly observe the change of the addendum thickness, it is advisable to select some values of Σ in its given range to draw the profile images on the axial section of the worm, as shown in Fig. 7.

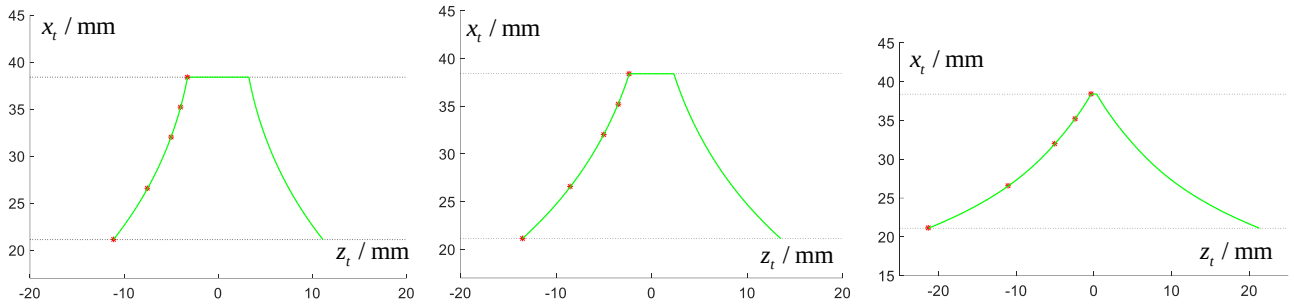

(a). $\Sigma = 9.79°$, $s_a = 6.51$mm (b). $\Sigma = 9.19°$, $s_a = 4.67$mm (c). $\Sigma = 8.39°$, $s_a = 0.71$mm

Fig. 7 Relationship between s_a and Σ

It can be clearly seen from Fig.7 (a)– (c) that with the decrease of the technological crossing angle Σ, the worm addendum thickness s_a also decreases gradually until the worm addendum becomes sharp. Generally, s_a should not less than $0.35m$ [7]. In Fig. 7 (c), $s_a < 0.35m$ is not meet thickness requirement. Therefore, the minimum value of Σ, $\Sigma_{\min}$, must be greater than $8.39°$. To obtain $\Sigma_{\min}$, a series of s_a can be obtained by taking different values of Σ based on the above calculation method, the data is shown in Table 4.

Table 4 Data of technological crossing angle and worm addendum thickness

Technological crossing angle Σ/°	9.79	9.59	9.39	9.19	8.99	8.79	8.59	8.39
Worm addendum thickness s_a / mm	6.51	5.96	5.35	4.67	3.9	3.0	1.97	0.71

Based on the data in Table 4, the method of polynomial interpolation fitting can be used to get the fitting curve of Σ and s_a / m, as shown in Fig. 8. The blue line is the fitting curve of Σ and s_a / m, and the red line parallel to the abscissa axis is the dividing line of the addendum thickness coefficient. The upper side of the red line is the value of Σ which satisfies the condition of the tooth thickness. It can be seen that the actual value range of Σ is smaller compared with the range calculated by Eq. (8).

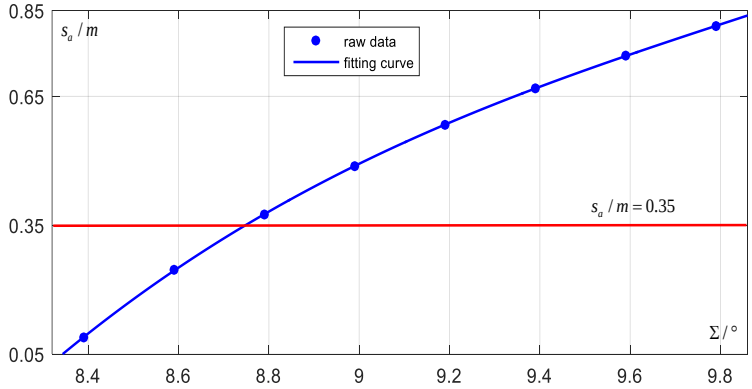

Fig. 8 Fitting curve of $\Sigma - s_a / m$ ($a = 200$mm, $i_{12} = 20$, $Z_1 = 2$)

Besides, the fitting model of the blue curve can be represented as $s_a / m = 0.07457\Sigma^3 - 2.209\Sigma^2 + 22.1557\Sigma - 74.3408$. The main evaluation parameters [20] of the fitting model are as follows: SSE: $7.71444*10^{-6}$, R-square: 1. Herein, the closer the value of SSE is to zero, the better the model selection and fitting, and the more successful the data prediction. And the closer the value of R-square is to 1, the stronger the explanatory ability of the Σ to s_a / m is. The results of these parameters show that the model is excellent for data fitting. According to this model, it can be calculated that when the addendum thickness coefficient of the worm is 0.35, the value of the

technological crossing angle is $8.75°$, which is the minimum value of Σ satisfying the addendum thickness condition. Thus, the feasible value range of Σ is $[8.75°,9.79°]$ in this example.

6 Computation on typical points of curvature interference limit line

To determining the key points of the curvature interference limit line, it can be assumed that the ordinate of the typical point is L_Ψ along the axis of the worm gear tooth surface, that is $z_2 = L_\Psi$. According to Eqs. (20), (21) and (28), a set of non-linear equations for solving the curvature interference limit line can be acquired as

$$z_2(\phi,\varphi,\varphi_1) = -y_{o1}^* = L_\Psi,\ \ \Phi(\phi,\varphi,\varphi_1) = 0,\ \ \Psi(\phi,\varphi,\varphi_1) = 0 \tag{38}$$

On the surface, the system of nonlinear Eqs (38) contains three independent unknowns ϕ, φ and φ_1. However, by further analyzing the characteristics of the equations, it can be found that parameter φ_1 only exists in the trigonometric function of the D-value between φ_1 and φ, and a single parameter φ only exists in the expression of z_{o1}. Therefore, for the convenience of calculation, ϕ, $\varphi_1-\varphi$ and z_{o1} can be regarded as the new unknowns of the system of equations (38). From the first two expressions of System (38), two equations can be expressed as $A\sin(\varphi_1-\varphi)+B\cos(\varphi_1-\varphi) = -C$, $-x_{o1}\sin(\varphi_1-\varphi) - y_{o1}\cos(\varphi_1-\varphi) = L_\Psi$. By means of Cramer's law and substituting the expressions of A, B and C into the first expression, it is possible to have the expressions of trigonometric function of $\varphi_1-\varphi$ as follows

$$\sin(\varphi_1-\varphi) = \frac{L_\Psi n_z x_{o1} + C y_{o1} - L_\Psi n_x z_{o1}}{(n_x x_{o1} + n_y y_{o1}) z_{o1} - n_z (x_{o1}^2 + y_{o1}^2)},\ \ \cos(\varphi_1-\varphi) = \frac{L_\Psi n_z y_{o1} - C x_{o1} - L_\Psi n_y z_{o1}}{(n_x x_{o1} + n_y y_{o1}) z_{o1} - n_z (x_{o1}^2 + y_{o1}^2)} \tag{39}$$

Equation (39) indicates that the trigonometric function value of $\varphi_1-\varphi$ can be represented by parameters z_{o1} and ϕ. According to $\sin^2(\varphi_1-\varphi)+\cos^2(\varphi_1-\varphi)=1$, a quadratic equation with respect to z_{o1} from Eq. (39) can be obtained as

$$a_z z_{o1}^2 + 2 n_z b_z z_{o1} + c_z = 0 \tag{40}$$

where $a_z = L_\Psi^2 (n_x^2 + n_y^2) - (n_x x_{o1} + n_y y_{o1})^2$, $b_z = \Delta_z (n_x x_{o1} + n_y y_{o1}) - p L_\Psi C$, $c_z = (x_{o1}^2 + y_{o1}^2)(C^2 - \Delta_z n_z^2)$ and $\Delta_z = x_{o1}^2 + y_{o1}^2 - L_\Psi^2$.

Eq. (40) leads up to

$$z_{o1} = \frac{A_z^{(i)} - n_z b_z}{a_z},\ \ i = 1,2 \tag{41}$$

where $A_z^{(i)} = (-1)^i \left| C(n_x x_{o1} + n_y y_{o1}) - p L_\Psi n_z^2 \right| \sqrt{\Delta_z}$, $i = 1,2$. It indicates that parameter z_{o1} is a single parameter function with regard to ϕ.

Substituting Eq. (41) into Eq. (39), the relationship between parameter ϕ and trigonometric function about $\varphi_1-\varphi$ can be obtained as below

$$\sin(\varphi_1-\varphi) = \frac{S_N}{D_T},\ \ \cos(\varphi_1-\varphi) = \frac{C_N}{D_T} \tag{42}$$

where $D_T = (n_x x_{o1} + n_y y_{o1})(A_z^{(i)} - n_z b_z) - n_z a_z (x_{o1}^2 + y_{o1}^2)$, $S_N = L_\Psi n_z a_z x_{o1} + C a_z y_{o1} - L_\Psi n_x (A_z^{(i)} - n_z b_z)$, $C_N = L_\Psi n_z a_z y_{o1} - C a_z x_{o1} - L_\Psi n_y (A_z^{(i)} - n_z b_z)$. Here, the values of symbols D_T, S_N and C_N are determined by the unique parameter ϕ.

In the light of Eqs. (41) and (42), the conclusion can be gained that parameter z_{o1} and trigonometric function of $\varphi_1-\varphi$ can be expressed by the one parameter ϕ. Next, the parameters z_{o1} and trigonometric function about $\varphi_1-\varphi$ will be replaced by parameter ϕ in the third equation of System (38) and the denominator containing parameter ϕ will be eliminated to avoid the influence of asymptote. It can be seen from Eqs. (17) and (25) that the symbols $\left(\vec{\boldsymbol{V}}_{12}\right)_{o1}\bullet\vec{\boldsymbol{g}}_1^{(1)}$, $\left(\vec{\boldsymbol{V}}_{12}\right)_{o1}^2$, n_{ox} and n_{oy} all contain the trigonometric function about $\varphi_1-\varphi$. Among them, the expressions of n_{ox} and n_{oy} are relatively simple, and they can be expressed directly by taking Eq (42) into them. The results are

$$n_{ox}=\frac{n_x C_N-n_y S_N}{D_T},\quad n_{oy}=\frac{n_x S_N+n_y C_N}{D_T} \tag{43}$$

In the process of calculating the point product of $\left(\vec{\boldsymbol{V}}_{12}\right)_{o1}$ and $\vec{\boldsymbol{g}}_1^{(1)}$, if their expressions adopt the final outcomes of Eqs. (19) and (23), the calculation process will be very complex and the obtained results cannot be simplified. Therefore, the expressions of vectors $\left(\vec{\boldsymbol{V}}_{12}\right)_{o1}$ and $\vec{\boldsymbol{g}}_1^{(1)}$ are selected as $\left(\vec{\boldsymbol{\omega}}_{12}\right)_{o1}\times\left(\vec{\boldsymbol{r}}_1^{*}\right)_{o1}-\left(\vec{\boldsymbol{\omega}}_2\right)_{o1}\times\left(\overrightarrow{O_2O_1}\right)_{o1}$ and $R\left[\vec{\boldsymbol{k}}_{o1},\varphi_1-\varphi\right]R\left[\vec{\boldsymbol{i}}_{o1},\Sigma\right]\left(\vec{\boldsymbol{g}}_1\right)_d$ respectively. Based on the knowledge of vector rotation [19], the expression of $\left(\vec{\boldsymbol{V}}_{12}\right)_{o1}\bullet\vec{\boldsymbol{g}}_1^{(1)}$ can be represented as

$$\left(\vec{\boldsymbol{V}}_{12}\right)_{o1}\bullet\vec{\boldsymbol{g}}_1^{(1)}=\frac{g_{1x}}{i_{12}}\left(z_{o1}-i_{12}y_{o1}^{*}\right)+g_{1y}x_{o1}^{*}+\frac{\sin\Sigma\cos\theta_0}{i_{12}}\left(a-x_{o1}^{*}\right) \tag{44}$$

According to Eq. (19), it is possible to have

$$\left(\vec{\boldsymbol{V}}_{12}\right)_{o1}^2=\frac{1}{i_{12}^2}\left(z_{o1}-i_{12}y_{o1}^{*}\right)^2+x_{o1}^{*\,2}+\frac{1}{i_{12}^2}\left(x_{o1}^{*}-a\right)^2 \tag{45}$$

Obviously, Eqs. (44) and (45) contain parameter z_{o1} and trigonometric function of $\varphi_1-\varphi$. Thus, substituting Eqs. (41), (42) and the expression $-y_{o1}^{*}=L_\Psi$ into Eqs. (44) and (45), the expressions of $\left(\vec{\boldsymbol{V}}_{12}\right)_{o1}\bullet\vec{\boldsymbol{g}}_1^{(1)}$ and $\left(\vec{\boldsymbol{V}}_{12}\right)_{o1}^2$ can be obtained as

$$\left(\vec{\boldsymbol{V}}_{12}\right)_{o1}\bullet\vec{\boldsymbol{g}}_1^{(1)}=\frac{1}{i_{12}a_z D_T}V_1,\quad \left(\vec{\boldsymbol{V}}_{12}\right)_{o1}^2=\frac{1}{i_{12}^2a_z^2 D_T}V \tag{46}$$

where $V_1=a_z\sin\Sigma\cos\theta_0\left(y_{o1}S_N-x_{o1}C_N\right)-\left(A_z^{(i)}-n_z b_z\right)\left(S_N\cos\Sigma\cos\theta_0+C_N\sin\theta_0\right)$

$$+a_z D_T\left[i_{12}\left(x_{o1}\cos\Sigma\cos\theta_0+y_{o1}\sin\theta_0\right)+a\sin\Sigma\cos\theta_0\right]$$

$$V=2D_T\left(A_z^{(i)}-n_z b_z\right)\left(i_{12}L_\Psi a_z-n_z b_z\right)-2aa_z^2\left(x_{o1}C_N-y_{o1}S_N\right)+a_z^2D_T\left[\Delta_z\left(i_{12}^2+1\right)+i_{12}^2L_\Psi^2+a^2\right]-a_z c_z D_T$$

Eventually, substituting Eqs. (41), (43) and (46) into Eq. (28), a nonlinear equation with one variable ϕ can be obtained as

$$f_\Psi(\phi)=\left(\rho g_{2z}\sin\Sigma\cos\theta_0-D_k\right)V_1^2+D_kD_TV+\rho D_k a_z D_T\left(A_z^{(i)}-n_z b_z\right)\left[n_z D_T-2i_{12}\left(n_x S_N+n_y C_N\right)\right]$$

$$+\rho D_k a_z^2 D_T\left\{\left[L_\Psi\left(n_x S_N+n_y C_N\right)-a\left(n_x C_N-n_y S_N\right)\right]+D_T\left(1+i_{12}^2\right)\left(n_x x_{o1}+n_y y_{o1}\right)\right\}=0,\ i=1,2 \tag{47}$$

In theory, given the value of L_Ψ, the corresponding value of ϕ can be obtained from Eq. (47). In fact, Eq. (47) is intricate, and it's hard to solve the unknown ϕ directly. Here, the method of the geometric drawing can be used to judge the existence of the solution of the equation. At the same time, according to the function image, an excellent initial value can be provided for iteration calculation

later. After obtaining the value of ϕ, other unknowns z_{o1} and $\varphi_1-\varphi$ can also be solved according to Eqs. (41) and (42). Then, the position of the typical point can be determined. By changing the value of L_Ψ, a series of typical points can be attained and the curvature interference limit line can be acquired by the interpolation method.

7 Analysis and discussion of numerical examples

7.1 Arrangement examples

It can be known from section 5.3 that the feasible value range of the technological crossing angle is $[8.75°,9.79°]$. In this section, the data in Tables 1 and 2 are taken as example A_1 to demonstrate the computing method of the curvature interference limit line. In example A_2, $\Sigma=9°$, $\Delta=280.4172\text{mm}$, $\theta_0=163.8373°$, and other parameters are the same as those in Tables 1 and 2. Compared with examples A_1 and A_2, the influence of Σ on interference limit line can be analyzed.

In addition, in order to fully understand the curvature interference characteristics of Litvin worm and avoid the chance of a single example. A new example is added. The main parameters are as follows: $a=120\text{mm}$, $i_{12}=15.5$, $Z_1=2$, $d_1=45\text{mm}$, $m=6$. Other parameters can be calculated from Tables 1 and 2. And its feasible value range of Σ is $[8.94°,10.08°]$. Herein, $\Sigma=10°$, $\Delta=59.5213\text{mm}$, $\theta_0=175.8178°$ is marked as example B_1. $\Sigma=9.5°$, $\Delta=171.6893\text{mm}$, $\theta_0=168.6788°$ is labeled as example B_2.

7.2 Computation results of numerical example

In order to elaborate the solution method of interference limit points, the values of L_Ψ are determined in example A_1 shown in Table 5. Based on the above computation method of curvature interference limit line, $L_\Psi=20$ can be selected as an instance to illustrate how to determine a typical point.

Table 5 Calculation results of typical points on curvature interference limit line of example A_1

Typical point	①	②	③	④	⑤	⑥	⑦	⑧	⑨	⑩
L_Ψ / mm	33.3	31.4	28	20	10	0	-10	-15	-15.7	-16.8
ϕ / °	-1.3650	-4.5556	-2.7654	2.1635	6.1232	8.1008	7.8089	6.2378	7.1955	11.6133
$(\varphi_1-\varphi)$ / °	-34.4605	-29.6294	-25.5711	-16.1181	-3.066	10.7046	24.5581	31.0123	32.4967	36.6582
z_{o1} / mm	70.0602	54.3312	-4.5031	-10.766	-13.7821	-13.1316	-7.6837	-1.1659	57.3645	70.7652
$\sqrt{x_{o1}^2+y_{o1}^2}$ / mm	47.9735	50.1729	48.9398	45.5365	42.8069	41.4496	41.6496	42.7281	42.0703	39.0544
z_{o2} / mm	33.3	31.4	28	20	10	0	-10	-15	-15.7	-16.8
$\sqrt{x_{o2}^2+y_{o2}^2}$ / mm	179.6874	169.7945	159.9249	159.4545	158.976	159.0933	159.7536	159.9956	170.8851	179.2992

Firstly, substituting $L_\Psi=20$ into Eq. (47), drawing its function image in given solution domain. Here, to avoid some meaningless points on the curve, the solution domain is reasonable given by $[-0.085,0.21]\text{rad}$. And then, draw its function image on account of MATLAB software, as shown in Fig. 9. The curve has an intersection point with the horizontal axis when $i=1$, and there is no intersection point when $i=2$. Therefore, the curve image of $i=1$ can be selected to compute the value of ϕ.

It can be seen from the local enlarged drawing that the intersection point between the abscissa and curve is in the neighborhood of the point $\phi=0.038$. On this occasion, substituting $\phi=0.038$ as the initial value into $f_\Psi=0$, an exact value of the parameter ϕ can be obtained by the iterative

method. Accordingly, the values of z_{o1} and $\varphi_1-\varphi$ can be solved based on Eqs. (41) and (42), and the parameter values on typical point of $L_\Psi=20$ are determined. Finally, by modifying the value of L_Ψ, other typical points can be determined. According to this, the curvature interference limit line can be acquired in accordance with the interpolation method.

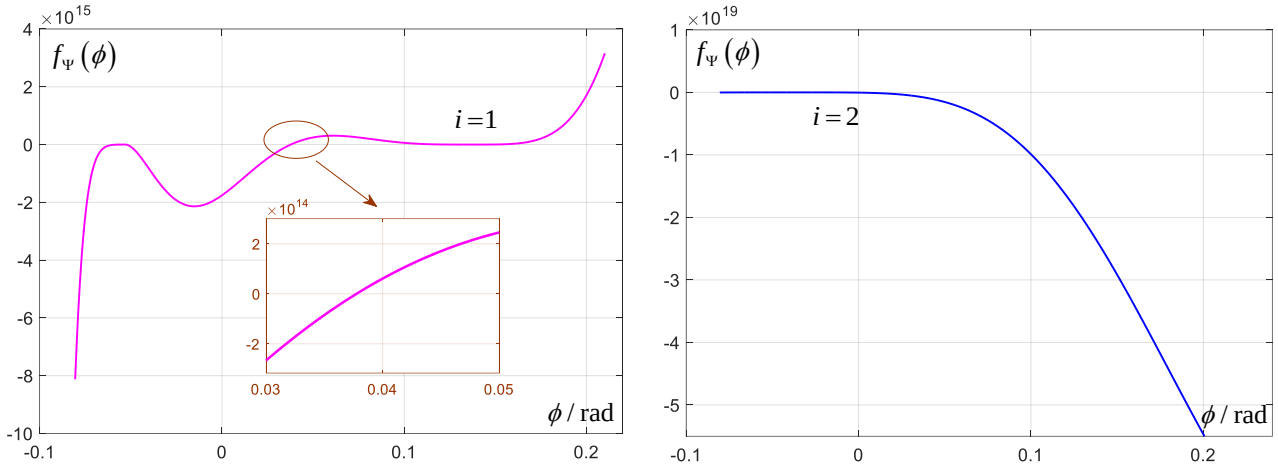

(a) $i=1$ (b) $i=2$

Fig.9 Curve image of function at the point $L_\Psi=20$

The curvature interference limit line is a space curve, so it is extremely difficult to direct observe its position relative to the worm gear tooth surface. For the purpose of demonstrating the position relationship between them, drawing its projection curves on the axial sections of the worm gear and worm, as shown in Fig. 10 (a) and (b), respectively. Besides, the computation results about the typical points of the curvature interference limit line on the surfaces of the worm gear and the gear are provided in Table 5.

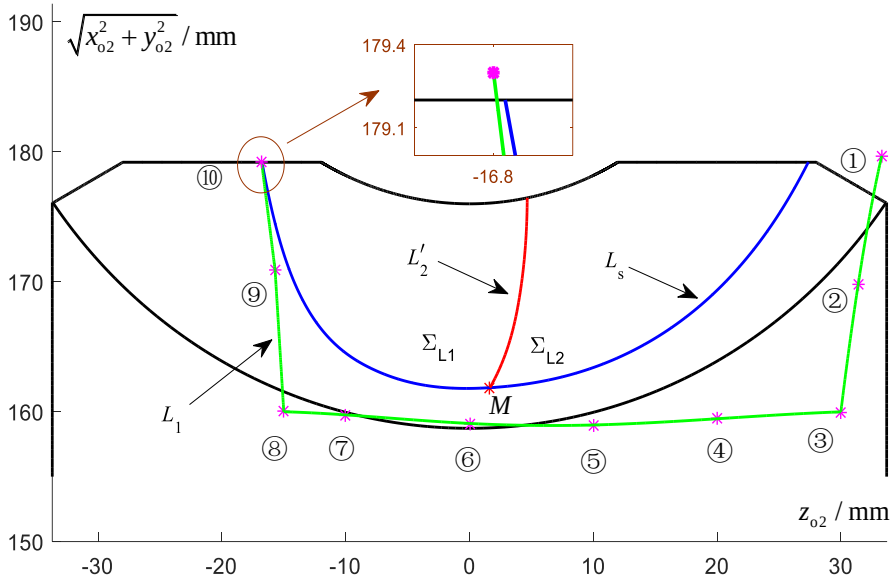

(a) Curvature interference limit line in axial section of tooth surface of worm gear

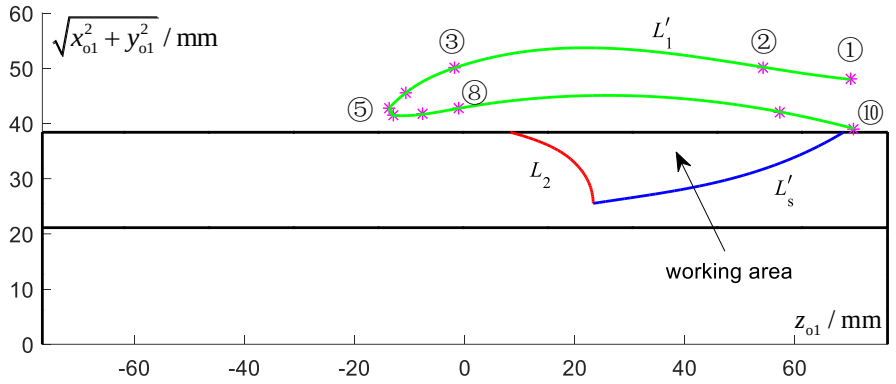

(b) Curvature interference limit line in axial section of worm

Fig.10. Curvature interference limit line of example A_1

In Fig. 10 (a), L_s is the projection line of the worm addendum on the tooth surface of the worm gear, namely, the boundary line of the conjugated area of the worm pair during the working meshing. L_2' is the conjugated line of the meshing limit line on the tooth surface of the worm gear, which divides the conjugate area of the worm gear tooth surface into two sub conjugate areas Σ_{L1} and Σ_{L2}. L_1 is the curvature interference limit line and the points ①~⑩ are the typical points on it. In Fig. 10 (b), L_s' is the projection line of the worm gear addendum on the tooth surface of the worm. L_2 is the meshing limit line. Because of its existence, the working length of the worm is always less than half of the total thread length. L_1' is the conjugated line of the curvature interference limit line on the worm helicoid. The area enclosed by lines L_2, L_s' and worm addendum line constitutes the working area of the worm.

As can be seen from Fig. 10 (a) that curvature interference limit line L_1 enters both sides of the worm gear tooth surface, especially the left side, but it does not enter the meshing area of the worm pair. Meanwhile, in Fig. 10 (b), the conjugated line L_1' of the interference limit line is located on the outside of the worm helicoid. On the other hand, the induced principal curvature of the curvature interference limit line is zero at any point. After calculation, the induced principal curvature at the point M is -0.0162. Since the direction of the unit normal vector of Σ_d is from the space points to the internal entity of the grinding wheel, which indicates that the point M is located on the side of no curvature interference. Thus, interference will not occur on the tooth surface of the worm gear in example A_1. Despite all this, Fig. 10 (a) and (b) show that there is a great risk of top cutting on the left side of the worm gear tooth surface, which needs to be given enough attention.

7.3 Influence of technological crossing angle on curvature interference limit line

Technological crossing angle Σ, as the most characteristic processing parameter compared with Niemann worm, is worth investigating. From the perspective of actual production and manufacturing, the main design parameters of the worm pair are given according to the design requirements and cannot be changed at will. On this occasion, it is easy to obtain better meshing performance by changing the value of Σ in its feasible range.

In this section, the influence of the technological crossing angle on the curvature interference limit line is studied. In examples A_2, B_1 and B_2, the positions of interference limit line in the axial sections of worm gear and worm are shown in Figs. 11, 12 and 13 respectively.

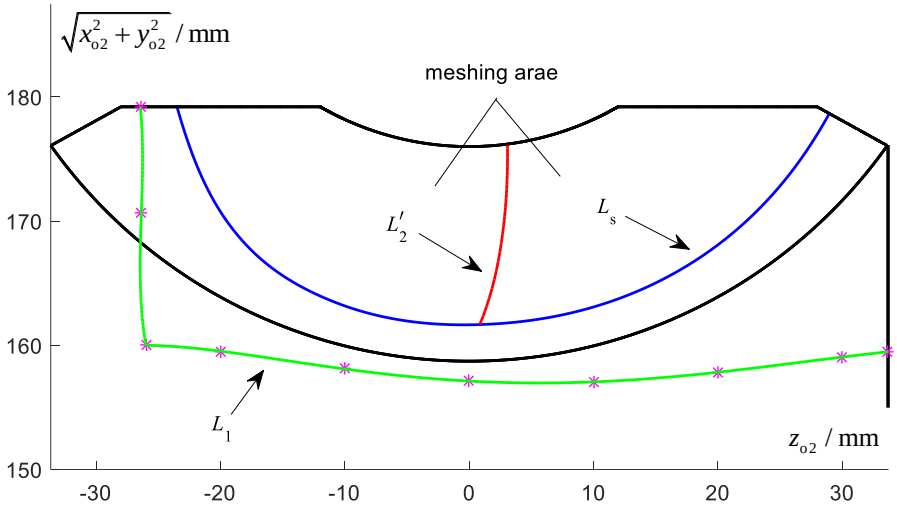

(a) Interference limit line on worm gear tooth surface

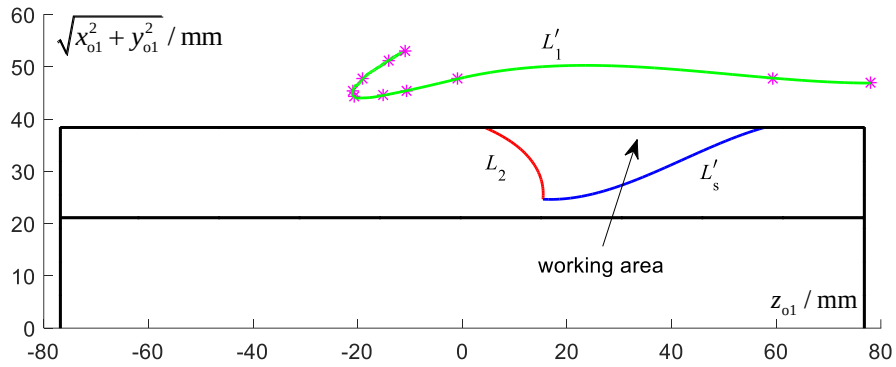

(b) Interference limit line in axial section of worm

Fig.11. Curvature interference limit line of example A_2

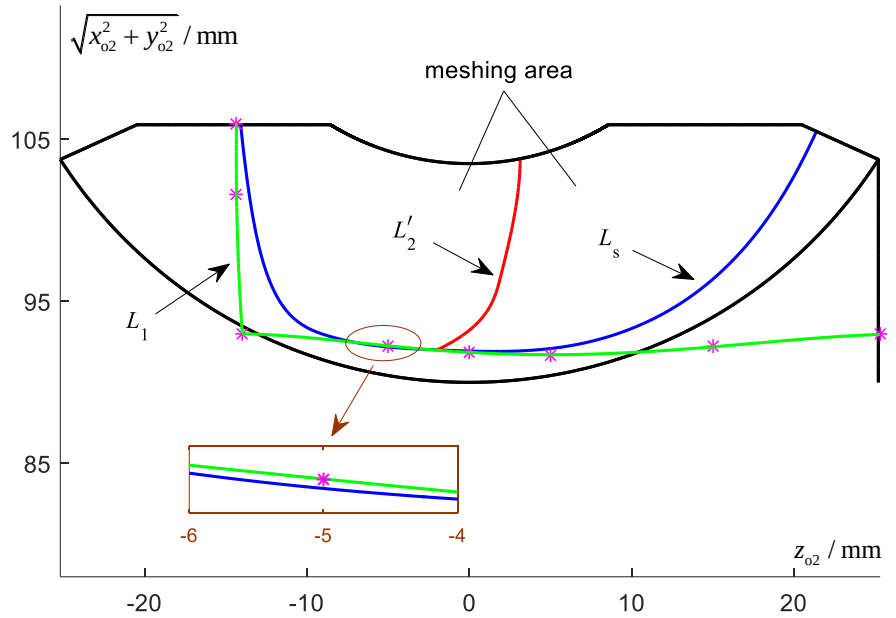

(a) Interference limit line on worm gear tooth surface

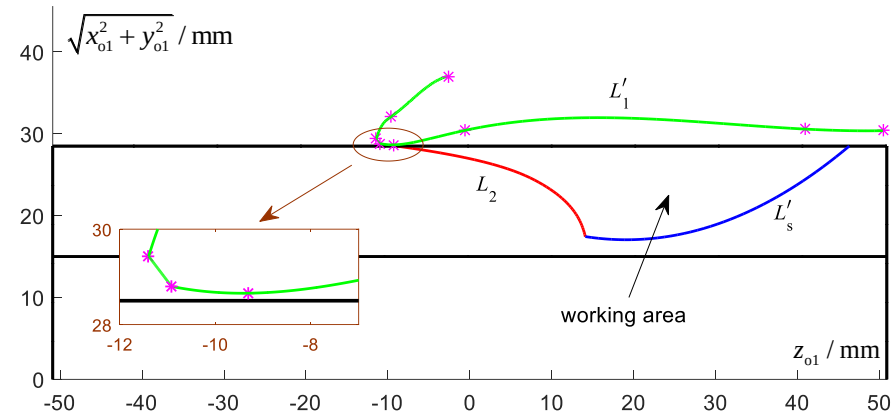

(b) Interference limit line in axial section of worm

Fig.12. Curvature interference limit line of example B_1

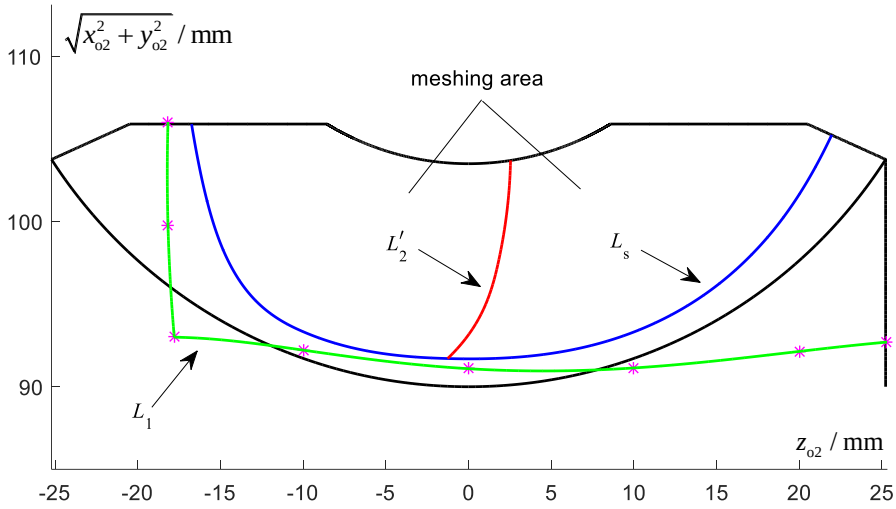

(a) Interference limit line on worm gear tooth surface

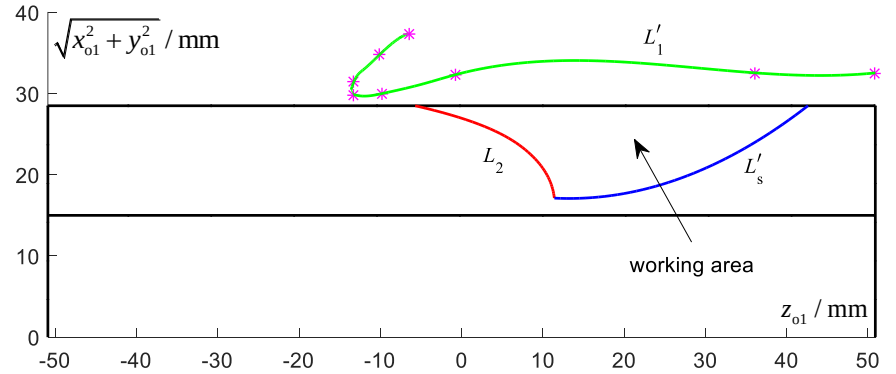

(b) Interference limit line in axial section of worm

Fig.13. Curvature interference limit line of example B_2

In Fig. 11 (a), although the interference limit line L_1 slightly enters the tooth surface of the worm gear, it doesn't cross the boundary line L_s of the meshing area, so the interference will not take place. Compared with Figs. 10 (a) and 11 (a), with the decrease of Σ, the meshing area of the worm pair increases significantly and the curvature interference limit line is far away from the boundary line L_s of the meshing area, which indicates that the risks of curvature interference decreased. Besides, from Figs. 10 (b) and 11 (b), it is obvious that the conjugated line L_1' is far away from the worm helicoid,

but the working length of the worm decreases slightly.

Compared with Figs. 12 and 13, the influence law of Σ on the curvature interference limit line is basically the same as the first group of examples. The difference is that undercutting occurs on the worm gear tooth surface in example B_1, as shown in Fig. 12(a). It can be clearly seen from the local enlarged drawing that the curvature interference limit line enters the meshing area of the worm gear tooth surface and is located on the upper side of the boundary line of the conjugated area L_s.

It can be concluded from the above examples that both top cutting and undercutting are possible for the proposed worm, especially undercutting. However, both problems can be solved by changing the value of the technological crossing angle.

8 Conclusions

The meshing theory of enveloping cylindrical worm drive with arc-toothed worm, especially the theory of curvature interference, is complete established. By building the mathematical models of grinding worm blank with grinding wheel and worm pair meshing, the equations of tooth surface, meshing function, meshing limit function and the curvature interference limit function are obtained.

The specific computation method of the tooth profile on the axial section of the worm is given. The relationship between the technological crossing angle and the worm addendum thickness is determined, and the result shows that there is a positive correlation between them. Besides, the worm addendum has become sharp before it is reduced to the lower limit value of the technological crossing angle. Based on curve fitting model of the technological crossing angle and addendum thickness coefficient , the feasible value range of the angle is obtained.

By observing the characteristics of equations of curvature interference limit line, the new unknowns which are easier to simplify the curvature interference equations are determined. And then the nonlinear equation with one parameter about the curvature interference limit line is obtained by elimination method. In the process of solving the zero point of the nonlinear equation, the existence of the solution of the equation is determined by using the geometric drawing method and a good initial value of iteration is also obtained. And finally, the projection curves of interference limit line on the tooth surfaces of worm and worm gear are obtained.

The results of numerical examples show that with the decrease of the technological crossing angle, the conjugated area of the worm gear tooth surface becomes larger, the working length of the worm decreases slightly, and the risk of interference decreases. So together, choosing a relatively small value of the technological crossing angle in its feasible value range can not only completely avoid the occurrence of interference, but also improve the meshing performance of the worm pair.

Conflict of interest

This work does not have any conflicts of interest.

Acknowledgements

This study was funded by the National Natural Science Foundation of China (52075083) and the Open Fund of the Key Laboratory for Metallurgical Equipment and Control of Education Ministry in Wuhan University of Science and Technology (2018B05 and MECOF2020B03).

ORCID

Xinyue Zhu https://orcid.org/0000-0001-7967-1066

References

1. Litvin FL, Fuentes A. *Gear geometry and applied theory*. 2nd ed. Cambridge: Cambridge University Press; 2004.
2. Willian P. Crosher. *Design and application of the worm gear*. New York: AMSE PRESS; 2002.
3. David B. Dooner. *Kinematic geometry of gearing*. 2nd ed. A John Wiley & Sons, Ltd., Publication; 2012.
4. Wang S. *New technology theory of ZC1 worm drive*. Tianjin: Tianjin University Press; 1992.
5. Litvin FL, Cheng Y. *A new type of cylindrical worm drive*. Shanghai: Shanghai Science and Technology Press, 1965.
6. Yuang ZJ, Liu HM. *Tool design handbook*. Machinery Industry Press; 1999.
7. Dong XZ. *Design and modification of toroidal worm drive*. Machinery Industry Press; 2004.
8. Wang SR, Liu PJ. *Meshing theory of cylindrical worm drive*. Tianjin: Tianjin Science and Technology Press; 1979.
9. Yang LC. *Circular tooth cylindrical worm drives*. Taiyuan: Shanxi People's Publishing House; 1984.
10. Chen X, Li J. Effect of the cutter parameters and machining parameters on the interference in gear slicing. *Chinese journal of mechanical engineering*. 2013; 26(6): 1118-1126.
11. Zhang YX, Qi L. *Design of worm drive Part 2 Design of circular cylindrical worm drive*. Beijing: Mechanical Industry Press; 1986.
12. Wang SR. *Circular cylindrical worm drives*. Tianjin: Tianjin University Press; 1990.
13. Zhao YP, Meng QX. Curvature interference characteristic of conical surface enveloping conical worm. *Forsch Ingenieurwes*. 2017: 81: 409–419. DOI:10.1007/s10010-017-0250-0.
14. Zhao YP, Meng QX. Curvature interference characteristic of conical worm gear. *Forsch Ingenieurwes*. 2019; 83: 759–773. DOI: 10.1007/s10010-019-00372-3.
15. Zhu RP, Gao DP. Study on the Method of Avoiding Dedendum Undercutting and Addendum Pointing in Face Gear Design. *Chinese Mechanical Engineering*, 1999; (11):82-84+7.
16. Cui YM, Fang ZD, Wang LP. Research on arc tooth face-gear with undercutting and pointing. *Mechanical Strength*, 2014; 36(04):572-577.
17. Meng QX, Zhao YP. Curvature Interference Characteristic of ZC1 Worm Gear. *New Approaches to Gear Design and Production*. 2020, 513-529. DOI: 10.1007/978-3-030-34945-5_24.
18. Chen WH. *Differential geometry*. 2nd ed. Beijing, Peking University Press, 2017.
19. Dong XZ. *Foundation of meshing theory for gear drives*. Beijing: China Machine Press; 1989.
20. Qu WX, Liu H, Qin C, et al. Antenna tracking accuracy evaluation method based on MATLAB Fourier curve fitting. *Electronic measurement technology*. 2020; 43(12):91-95.